The Astrophysical Journal, 740:20 (18pp), 2011 October 10 doi:10.1088/0004-637X/740/1/20

THE VLA SURVEY OF CHANDRA DEEP FIELD SOUTH. V. EVOLUTION AND LUMINOSITY FUNCTIONS OF SUB-MILLIJANSKY RADIO SOURCES AND THE ISSUE OF RADIO EMISSION IN RADIO-QUIET ACTIVE GALACTIC NUCLEI

P. Padovani[1], N. Miller[2], K. I. Kellermann[3], V. Mainieri[1], P. Rosati[1], and P. Tozzi[4]
[1] European Southern Observatory, D-85748 Garching bei München, Germany; ppadovan@eso.org
[2] Department of Astronomy, University of Maryland, College Park, MD 20742-2421, USA
[3] National Radio Astronomy Observatory, Charlottesville, VA 22903-2475, USA
[4] INAF, Osservatorio Astronomico di Trieste, I-34131, Trieste, Italy
Received 2011 March 3; accepted 2011 July 11; published 2011 September 21

ABSTRACT

We present the evolutionary properties and luminosity functions of the radio sources belonging to the Chandra Deep Field South Very Large Array survey, which reaches a flux density limit at 1.4 GHz of 43 μJy at the field center and redshift $\sim$5 and which includes the first radio-selected complete sample of radio-quiet active galactic nuclei (AGNs). We use a new, comprehensive classification scheme based on radio, far- and near-IR, optical, and X-ray data to disentangle star-forming galaxies (SFGs) from AGNs and radio-quiet from radio-loud AGNs. We confirm our previous result that SFGs become dominant only below 0.1 mJy. The sub-millijansky radio sky turns out to be a complex mix of SFGs and radio-quiet AGNs evolving at a similar, strong rate; non-evolving low-luminosity radio galaxies; and declining radio powerful ($P \gtrsim 3 \times 10^{24}$ W Hz^{-1}) AGNs. Our results suggest that radio emission from radio-quiet AGNs is closely related to star formation. The detection of compact, high brightness temperature cores in several nearby radio-quiet AGNs can be explained by the coexistence of two components, one non-evolving and AGN related and one evolving and star formation related. Radio-quiet AGNs are an important class of sub-millijansky sources, accounting for $\sim$30% of the sample and $\sim$60% of all AGNs, and outnumbering radio-loud AGNs at $\lesssim$0.1 mJy. This implies that future, large area sub-millijansky surveys, given the appropriate ancillary multiwavelength data, have the potential of being able to assemble vast samples of radio-quiet AGNs, bypassing the problems of obscuration that plague the optical and soft X-ray bands.

Key words: galaxies: active – galaxies: starburst – infrared: galaxies – radio continuum: galaxies – X-rays: galaxies

Online-only material: color figures

1. INTRODUCTION

The relationship between star formation and active galactic nuclei (AGNs) in the universe is one of the hottest topics of current extragalactic research, at two different levels. On cosmological scales, the growth of supermassive black holes in AGNs appears to be correlated with the growth of stellar mass in galaxies (e.g., Merloni et al. 2008). On nuclear scales, the accreting gas feeding the black hole at the center of the AGN might trigger a starburst. The black hole, through winds and jets, can in turn feed energy back to its surroundings, which can compress the gas and therefore accelerate star formation but can also blow it away, thereby stopping accretion and star formation altogether. The general consensus is that nuclear activity plays a major role in the co-evolution of supermassive black holes and galaxies through the so-called AGN Feedback, and indeed radio emission from AGNs has been recently suggested to play an important role in galaxy evolution (Croton et al. 2006). Moreover, radio observations afford a view of the universe unaffected by the absorption, which plagues observations made at most other wavelengths, and therefore provide a vital contribution to our understanding of this co-evolution. These two points imply that studies of the evolution of star-forming galaxies (SFGs) and AGNs in the radio band should provide a better understanding of the link between the two phenomena. These are obviously done best by reaching relatively faint ($\lesssim$1 mJy) flux densities, and hence the importance of characterizing the radio faint source population.

After years of intense debate, the contribution to the sub-millijansky population from synchrotron emission resulting from relativistic plasma ejected from supernovae associated with massive star formation in galaxies appears not to be overwhelming, at least down to $\sim$50 μJy, contrary to the (until recently) most accepted paradigm. Our deep ($S_{1.4\,\mathrm{GHz}} \geqslant 43$ μJy) radio observations with the NRAO Very Large Array (VLA) of the Chandra Deep Field South (CDFS), complemented by a variety of data at other frequencies, imply in fact a roughly 50/50 split between SFGs and AGNs (Padovani et al. 2009), in broad agreement with other recent papers (e.g., Seymour et al. 2008; Smolčić et al. 2008).

The purpose of this paper is to study the evolution and luminosity functions (LFs) of sub-millijansky radio sources through the VLA-CDFS sample. Apart from the topics mentioned above, this is important also for other issues, including:

1. predictions for the source population at radio flux densities <1 μJy, which are relevant, for example, for the Square Kilometre Array (SKA). All existing estimates, in fact, had to rely, for obvious reasons, on extrapolations and are based on high flux density samples. This particularly affects the highest redshifts, which can be probed better at fainter flux densities;
2. the radio evolution of radio-quiet AGNs. No radio-selected sample of radio-quiet AGNs is currently available and this is badly needed to shed light on the mechanism behind their radio emission and allow a proper comparison with radio-loud quasars; and
3. the fact that number counts by themselves do not necessarily reflect the relative intrinsic abundance of astrophysical sources, which requires the determination of the evolution and LF (Padovani et al. 2007).

We note that the evolution and LFs of sub-millijansky radio sources have been studied, so far, only in two fields: the Cosmological Evolution Survey (COSMOS) field (Smolčić et al. 2009a, 2009b) and the Deep *Spitzer* Wide-area InfraRed Extragalactic (SWIRE) field (Strazzullo et al. 2010), in both cases up to a maximum redshift of 1.3 and without differentiating between radio-quiet and radio-loud AGNs. Source classification was based on a rest-frame optical color scheme and on spectral energy distribution (SED) fitted to photometric data covering the UV-to-near-IR range, respectively.

We define AGN sources in which most of the energy is produced through physical processes other than the nuclear fusion that powers stars. In practice, this means that electromagnetic emission most likely related, directly or indirectly, to a supermassive black hole is predominant in at least one band. A small fraction of AGNs have, for the same optical power, radio powers three to four orders of magnitude higher than the rest. These are called "radio-loud" quasars and most of the energy they emit is non-thermal and is associated with powerful relativistic jets, although thermal components associated with an accretion disk may also be observed, especially in the optical/UV band. Radio galaxies are also characterized by strong radio jets (manifested also through radio lobes), typically laying in or near the plane of the sky, and a fraction of them (the most powerful ones) are thought to be radio-loud quasars, which have instead their jets oriented with a small angle to the line of sight (e.g., Urry & Padovani 1995). We define as "radio-quiet" AGNs in which jets are either not present or make a tiny contribution to the total energy budget over the whole electromagnetic spectrum, which is dominated by thermal emission. All other AGNs we call radio-loud. Note that radio-quiet AGNs are not radio-silent. Indeed, the radio power of many low-luminosity radio galaxies, the so-called Fanaroff–Riley (FR) Is ("low-power radio-loud AGNs" according to our nomenclature) overlap with that of radio-quiet AGNs, which can generate some confusion and requires great care during the classification process, which needs to involve also the X-ray and far-IR bands (Section 2.4). However, the two classes are physically distinct (see Sections 5.3 and 5.8), although the origin of radio emission in radio-quiet AGNs is still not clear (but see Section 5.7).

Translating these high-level definitions into a classification scheme requires a wealth of multiwavelength data, which were described in our previous papers. Kellermann et al. (2008, Paper I) presented the radio data of the VLA-CDFS sample, together with optical images and X-ray counterparts, while Mainieri et al. (2008, Paper II) discussed the optical and near-IR counterparts to the observed radio sources and, based on rest-frame colors and the morphology of the host galaxies, found evidence for a change in the sub-millijansky radio source population below $\approx$80 μJy. Tozzi et al. (2009, Paper III) dealt with the X-ray properties, while Padovani et al. (2009, Paper IV) discussed the source population. This turned out to be made up of SFGs and AGNs at roughly equal levels, with the AGN including radio galaxies, mostly low-power (FR Is), and a significant ($\sim$50%) radio-quiet component. Paper IV made also clear that the "standard" definitions of radio-loudness, based on radio-to-optical flux density ratios, R, and radio powers, were insufficient to identify radio-quiet AGNs when dealing with a sample, which included also star-forming and radio-galaxies, as both classes are or can be (respectively) characterized by low R and radio powers as well. R, for example, is useful for quasar samples, where it can be assumed that the optical flux is related to the accretion disk, but obviously loses its meaning as an indicator of jet strength if both the radio and the optical bands are dominated by jet emission, as might be the case in FR Is (Chiaberge et al. 1999). Source classification in Paper IV was then based on radio, optical, and X-ray data, and was meant to provide a robust upper limit to the fraction of SFGs at sub-millijansky levels. SFG candidates were selected based on their (low values of) R, (low) radio power, (non-elliptical or S0) optical morphology, and (low) X-ray power ($L_{\rm x}$). The fact that X-ray upper limits above the AGN threshold (10^{42} erg s^{-1}) were also included was conservative in the sense that it maximized the number of SFGs, as some of these sources could still be AGNs. Furthermore, the selection of radio-quiet AGN candidates was only approximate, as it was based solely on R and $L_{\rm x}$ and suffered from uncertainties in the optical K-correction, possible contamination by radio galaxies, and the exclusion of X-ray upper limits (see Paper IV for details). In order to deal with the evolution and luminosity functions of the various classes of sources, we need to refine our classification. In particular, the CDFS field has been observed by *Spitzer* and therefore near- (Section 2.2) and mid/far-IR (Section 2.3) data are available for our sample. The source classification used in this paper relies then on a combination of radio, IR, optical, and X-ray data (Section 2.4).

Section 2 describes the updated classification of the VLA-CDFS sample, while Section 3 studies its evolution. Section 4 derives the LFs for various classes, while Section 5 discusses our results. Finally, Section 6 summarizes our conclusions. Throughout this paper spectral indices are defined by $S_\nu \propto \nu^{-\alpha}$ and the values $H_0 = 70$ km s^{-1} Mpc^{-1}, $\Omega_{\rm M} = 0.3$, and $\Omega_\Lambda = 0.7$ have been used.

2. THE UPDATED SAMPLE CLASSIFICATION

2.1. Redshifts

Our sample includes all VLA-CDFS sources with reliable optical counterparts and eight empty fields, for total of 256 objects, 193 of which belong to a complete sample[5] (see Paper IV for details). 92% of the sources in the complete sample now have redshift information (74% spectroscopic) as compared to only 77% in Paper IV. We have included in this paper spectroscopic redshifts from a dedicated follow-up program performed with the VIMOS spectrograph at the Very Large Telescope (M. Bonzini et al. 2011, in preparation). We also used recently published redshifts for the counterparts of *Chandra* sources in this field (Treister et al. 2009; Silverman et al. 2010) and the photometric redshifts published by the Multiwavelength Survey by Yale-Chile (MUSYC; Cardamone et al. 2010), which are based on 32 photometric bands.

As shown in Figure 1, redshift is strongly correlated with magnitude, albeit with some scatter. The best and simplest approach to estimate the redshift for the 16 objects in the complete sample without observed redshifts is then to derive it from their magnitude by using the relationship shown in the figure (solid line), that is $\log z = 0.166 V_{\rm mag} - 3.85$. This was derived applying to the whole sample the ordinary least-squares bisector method (Isobe et al. 1990), which treats the variables symmetrically. Including only spectroscopic redshifts, or only the complete sample, or excluding sources with likely AGN contamination in the optical band (based on Szokoly et al. 2004),

[5] Four more sources belonging to the complete sample have very uncertain counterparts (see Paper II) and for one other source, very close to a bright star, we could not get reliable photometry. The inclusion of these sources in any of the classes described below would change our results by much less than 1σ.

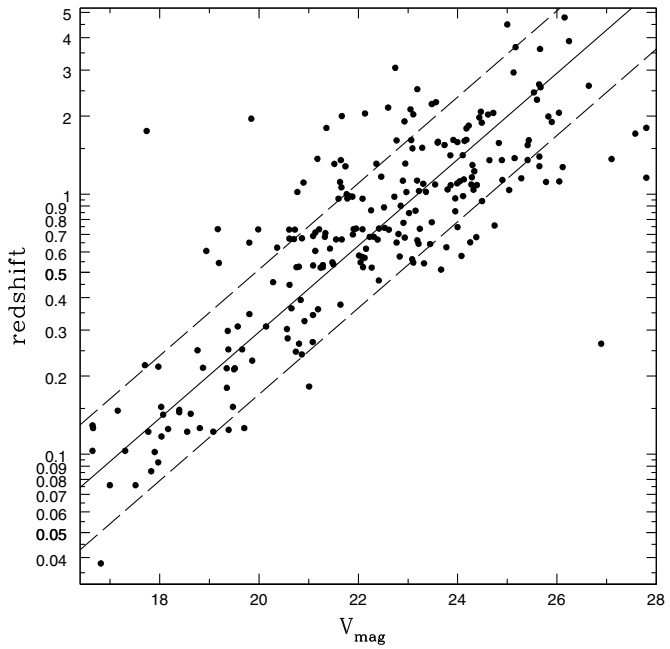

Figure 1. Redshift vs. $V_{\rm mag}$ for our sources with redshift information. The solid line is the best fit, while the dashed lines represent the scatter. See the text for details.

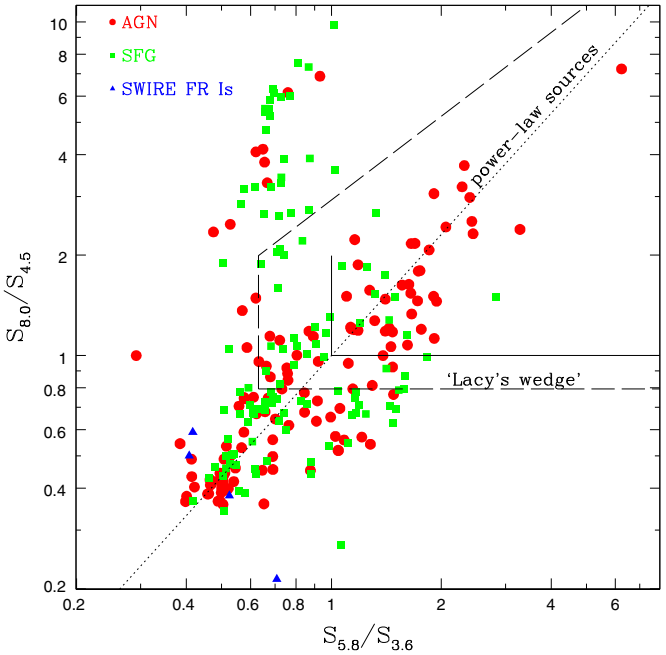

Figure 2. IRAC color–color plot for the AGN and SFG candidates selected in Paper IV and four FR Is from the SWIRE field. The dotted line indicates the locus of sources whose spectrum can be described as a power law over the four IRAC bands. The dashed lines indicate the so-called Lacy's wedge, which is where most AGNs are thought to lie. The solid lines denote a more restrictive region, which takes into account the fact that for $z > 0.5$, PAH- and star-light-dominated sources can be inside "Lacy's wedge" (Dasyra et al. 2009). See the text for details.

(A color version of this figure is available in the online journal.)

all give relations within 1σ from the adopted one. The effect of this assumption on our results is discussed in Section 5.1.

Note that while objects well to the left of the correlation can be explained as having an AGN component in the optical band, the single source in the lower right part of the diagram is ≈7 mag fainter than the average and therefore well into the dwarf galaxy regime. However, its photometry is affected by its closeness to a bright star, which might explain at least in part its faintness.

2.2. Near-IR Data

The usage of the *Spitzer* Infrared Array Camera (IRAC; Fazio et al. 2004) colors to identify AGNs has been discussed at length in the literature (e.g., Lacy et al. 2004; Hatziminaoglou et al. 2005; Stern et al. 2005; Sajina et al. 2005; Cardamone et al. 2008). Although it is by now evident that only some classes of extragalactic sources occupy restricted regions of parameter space in such plots, it is nevertheless also clear that there are broad trends which can be used to, for example, identify possible misclassifications.

Figure 2 plots the IRAC flux density ratios $S_{8.0}/S_{4.5}$ versus $S_{5.8}/S_{3.6}$ for our sources classified as in Paper IV, where the flux densities refer to all four IRAC channels at 3.6, 4.5, 5.8, and 8.0 μm. The IRAC data come from the *Spitzer* IRAC/MUSYC Public Legacy survey in the Extended CDFS (SIMPLE; Damen et al. 2011). We cross-correlated the SIMPLE catalog with the VLA-CDFS sources, accepting matches with separations less than $2''$. The SIMPLE catalog has convolved the images associated with each IRAC channel to match that of channel 4 (8.0 μm), the one with the lowest resolution, so that reasonably accurate colors may be obtained from the four IRAC bands. We have used total fluxes and applied the prescribed normalization to produce flux densities in μJy. Figure 2 shows the following: (1) most AGN candidates fall around the locus of sources whose mid-IR spectrum can be characterized by a single power law (dotted line); a significant number of AGNs is also within the so-called Lacy's wedge (dashed lines), which is where most unobscured, broad-lined (type 1) AGNs are thought to lie (Lacy et al. 2004). Note that highly obscured sources might also occupy that region of parameter space (e.g., Dasyra et al. 2009; Prandoni 2010); (2) most SFG candidates are distributed in a vertical band centered around $S_{5.8}/S_{3.6} \sim 0.6$–0.8, which is where polycyclic aromatic hydrocarbon (PAH)- and starlight-dominated sources are expected to lie (e.g., Sajina et al. 2005); (3) we also plot four "bona fide" FR Is from the SWIRE field (Vardoulaki et al. 2008), which fall in the region where galaxies with an old stellar population are located (e.g., Sajina et al. 2005). We have quite a few sources in the same area, which is consistent with one of the main results of Paper IV, that is, the dominance of low-luminosity radio galaxies among radio-loud AGNs.

This is reassuring and shows that the SFG/AGN division derived in Paper IV is overall correct. The most interesting features in Figure 2, however, are the exceptions to the above, namely:

1. The eight AGN candidates in the top left part of the diagram; these are all but one low redshift ($z \leqslant 0.25$), low radio power ($\log P_{1.4\rm GHz} \leqslant 22.6$), low X-ray (2–10 keV) power ($\log L_{\rm x} \leqslant 41.6$) sources, which had been classified as AGNs solely because their optical morphology was S0 (5) or elliptical. A closer look at their images shows that two of them show (weak) signs of spiral arms and four more (all S0) have only low-resolution Wide Field Imager (WFI) data, which means that the presence of spiral arms cannot be excluded. Their location in the PAH-dominated region (Sajina et al. 2005) suggests a re-classification as SFGs for all of them apart from one AGN with two spiral galaxies at a distance of $\sim 3''$, which means its IRAC flux is most likely contaminated (its rest-frame radio-to-optical flux density

ratio is also ∼2, which is typical of radio-loud AGNs: see below).

2. The 10 SFG candidates with $S_{5.8}/S_{3.6} > 1$ and $1 < S_{8.0}/S_{4.5} < 3$; this is more restrictive than the Lacy's wedge as it takes into account the fact that for $z > 0.5$ PAH- and star-light-dominated sources can be inside that wedge (Dasyra et al. 2009). Most of these sources have X-ray upper limits larger than 10^{42} erg s^{-1}, which makes sense since this was one of the reasons they were classified as SFGs in the first place. The location of these sources suggests a re-classification as AGNs.

In summary, seven sources were re-classified from AGNs to SFGs and ten sources previously classified as SFGs are now classified as AGNs.

2.3. Far-IR Data

It is well known that the global far-IR and radio emission are tightly and linearly correlated in star-forming systems (e.g., Sargent et al. 2010 and references therein). This is usually expressed through the so-called q parameter, that is, the logarithm of the ratio of far-IR to radio flux density, as defined by Helou et al. (1985). We take advantage of the relatively narrow dispersion of q for star-forming systems to further refine our SFG/AGN separation and also to improve on our radio-quiet–radio-loud AGN division, as the latter does not follow the IR–radio correlation typical of SFGs (e.g., Sopp & Alexander 1991; Sargent et al. 2010). This is vital to separate radio-quiet AGNs from radio galaxies, as R is not very useful in this case (Section 1) and, like radio-quiet AGNs, radio galaxies can also have relatively large X-ray powers.

We have used a catalog of 70 μm Multiband Imaging Photometer for *Spitzer* (MIPS) flux densities from the Far-infrared Deep Extragalactic Survey (FIDEL; M. Dickinson et al. 2011, in preparation) for our evaluation of q. We cross-correlated the VLA-CDFS radio sources with the FIDEL catalog using a radius of 8″ (about half the *Spitzer* 70 μm point-spread function). For those sources undetected by the FIDEL survey (but still within the FIDEL coverage), we assume an upper limit of 2.5 mJy as this is approximately the 5σ survey limit. To these data we add 24 μm flux densities from the Great Observatories Origins Deep Survey (GOODS) whenever available, and thus we obtain SEDs sampled at up to eight wavelengths: 20 and 6 cm in the radio from our VLA surveys; 70 μm and 24 μm in the IR from FIDEL and GOODS; and 8.0 μm, 5.6 μm, 4.5 μm, and 3.6 μm in the near-IR from SIMPLE.

We then proceeded to find the template SED from the Dale et al. (2001) SFG models that best matches the *Spitzer* data. We use the source redshifts to place each of the 64 models into the observed frame for that source, and set the normalization by requiring that each model SED pass through the measured 70 μm flux density for that galaxy. This, in effect, places an extra weight on 70 μm data since it is our only measurement of the smooth modified blackbody portion of the SED. We then select the model that minimizes the least-squares fit to the photometry of the four IRAC channels and the MIPS 24 μm data (when available). Once the best-fitting model has been selected, we derive the rest-frame 60 μm and 100 μm flux densities to determine FIR, the total far-IR flux between 42.5 μm and 122.5 μm (Helou et al. 1985):

$$\mathrm{FIR} = 1.26 \times 10^{-14}\,[2.58\,f_{60\mu\mathrm{m}} + f_{100\mu\mathrm{m}}]\,\mathrm{W\,m^{-2}}, \quad (1)$$

where the flux densities, f, are in Jy. Similarly, we convert the observed 1.4 GHz radio emission to the rest frame by using its measured spectral index between 1.4 GHz and 4.86 GHz, where available (∼80% of the sample: see Paper I), or otherwise assuming a spectral index $\alpha_\mathrm{r} = 0.7$ (the mean of the sample). The value of q is then calculated as the logarithm of the ratio of far-IR to 1.4 GHz flux density:

$$q = \log\,[(\mathrm{FIR}/3.75 \times 10^{12})/S_{1.4\,\mathrm{GHz}}], \quad (2)$$

where the numeric factor is the frequency in Hz corresponding to a wavelength of 80 μm.

Given the large fraction (∼50%) of upper limits on q, one cannot readily look for a bimodality in its distribution to define a dividing line between star-forming and non-star-forming sources. The median of the detections should be however quite well defined, as its value is 2.16 and most upper limits are below 2.2. Since 96% of the detections above the median are below 2.64 and assuming a symmetric distribution, one finds a lower end at around $2.16 - (2.64–2.16) \sim 1.7$. We then assume in the following that sources characterized by $q \geqslant 1.7$ are star-formers[6] (upper limits above this value excluded). This is the same dividing value assumed by Machalski & Condon (1999). Twenty-two of our candidate SFGs have $q < 1.7$ and therefore cannot be star-forming systems. These were then re-classified as radio-loud AGNs. These sources fall in the region where passive galaxies are found in the IRAC color–color plot, which is consistent with this re-classification, given that most of our radio-loud AGNs should be radio galaxies.

Finally, eight radio-quiet AGN candidates were found to have $q < 1.7$, while nineteen radio-loud ones had $q \geqslant 1.7$, which reflects the approximation of our previous classification. These objects were re-classified as radio-loud and radio-quiet, respectively.

2.4. Revised Classification

To summarize, based on the results presented in Paper IV and in the previous sub-sections, our candidate SFGs are defined as fulfilling the following initial requirements:

1. $R = \log(S_{1.4\mathrm{GHz}}/S_\mathrm{V}) < 1.7$ (where S_V is the V-band flux density),
2. $P_\mathrm{r} < 10^{24.5}$ W Hz^{-1},
3. optical morphology different from elliptical or lenticular, and
4. $L_\mathrm{x}(2–10\,\mathrm{keV}) < 10^{42}$ erg s^{-1} for X-ray detections, no limit otherwise.

As discussed in Paper IV, the first two criteria include ∼90% of spirals and irregulars, and the third one excludes sources not associated with star formation at our redshifts ($\langle z \rangle \sim 1.1$), while the fourth one excludes AGNs. These are then supplemented by the following additional requirements, which can overrule the previous ones if necessary:

5. IRAC constraints: the region of parameter space defined by $S_{5.8}/S_{3.6} > 1$ and $1 < S_{8.0}/S_{4.5} \lesssim 3(S_{5.8}/S_{3.6})^{0.83}$ (AGN region) is excluded; sources not classified as SFGs by the previous criteria but with $0.45 < S_{5.8}/S_{3.6} < 1.0$ and $S_{8.0}/S_{4.5} > 2.3$ (PAH-dominated region) are also included (Section 2.2);
6. MIPS constraints: $q \geqslant 1.7$, upper limits above this value excluded (Section 2.3).

[6] Our results are only weakly dependent on this choice. For example, if we defined as star-formers sources with $q \geqslant 1.8$ our SFG complete sample would only lose three objects, a 4% effect (see Table 2).

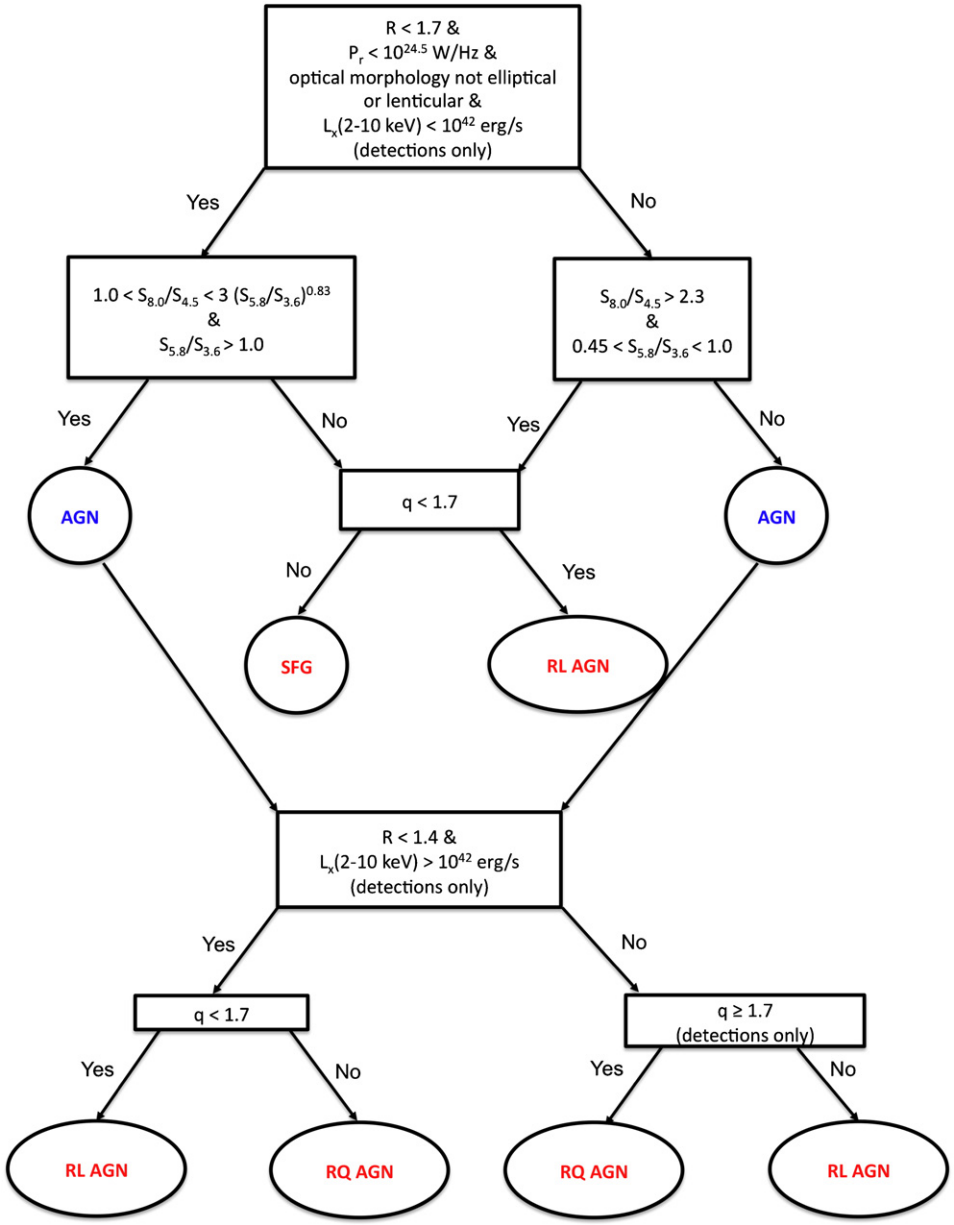

Figure 3. Flow chart of our classification scheme. See the text for details.
(A color version of this figure is available in the online journal.)

Note that constraints numbers 2 and 3 have become almost irrelevant for our classification given these two new requirements. Objects not fulfilling this sequence of criteria are considered to be AGNs. Radio-quiet AGNs are defined initially as follows:

1. $R < 1.4$, and
2. $L_{\rm x}(2\text{–}10\,{\rm keV}) > 10^{42}$ erg s^{-1} (detections only).

As discussed in Paper IV, the first criterion is the "classical" definition of radio-quiet AGNs converted to the 1.4 GHz and V bands. These are then supplemented by the following additional requirements, which can overrule the previous ones if necessary:

3. IRAC constraints: the region of parameter space defined by $S_{8.0}/S_{4.5} > 2.3$ and $0.45 < S_{5.8}/S_{3.6} < 1.0$ (PAH-dominated region) is excluded (Section 2.2); and
4. MIPS constraints: $q \geqslant 1.7$, upper limits above this value excluded (Section 2.3).

AGNs not fulfilling this sequence of criteria are considered to be radio-loud. Figure 3 summarizes our classification scheme. We note that, while it is relatively simple to distinguish SFGs from radio-loud AGNs due to their different q values, the situation is more complicated when one has to differentiate SFGs from radio-quiet AGNs. This is done also based on the location on the IRAC color–color plot, which highlights the obvious outliers, but mostly on the basis of X-ray power. Since many SFGs still have upper limits on $L_{\rm x}(2\text{–}10\,{\rm keV}) > 10^{42}$ erg s^{-1}, we cannot exclude the possibility that more radio-quiet AGNs are present in our sample, especially among the SFG with the highest limits on $L_{\rm x}(2\text{–}10\,{\rm keV})$, which tend to be at higher redshifts. The inclusion of deeper X-ray data in our analysis will help us sort out this issue.

It is instructive to see how representative local sources get classified by our scheme. To this aim, we have used the NASA/IPAC Extragalactic Database (NED) and NASA's Astrophysics Data System (ADS) to get multiwavelength data for a few objects. For example, NGC 1068, the prototype Seyfert 2 galaxy, residing in a spiral host, has low R, $P_{\rm r}$, and $L_{\rm x}(2\text{–}10\,{\rm keV})$

Table 1
Euclidean Normalized 1.4 GHz Counts

Flux Range (μJy)	Mean Flux Density (μJy)	Total (sr^{-1} $Jy^{1.5}$)	SFG (sr^{-1} $Jy^{1.5}$)	Fraction (%)	Counts AGN (sr^{-1} $Jy^{1.5}$)	Fraction (%)	RL AGN	RQ AGN
43–75	63	$2.53^{+0.51}_{-0.42}$	$1.49^{+0.40}_{-0.32}$	59^{+18}_{-17}	$1.03^{+0.37}_{-0.28}$	41^{+16}_{-14}	$0.16^{+0.16}_{-0.09}$	$0.87^{+0.37}_{-0.27}$
75–120	97	$2.62^{+0.45}_{-0.38}$	$1.33^{+0.34}_{-0.28}$	51^{+15}_{-14}	$1.24^{+0.32}_{-0.26}$	47^{+14}_{-13}	$0.60^{+0.24}_{-0.18}$	$0.64^{+0.26}_{-0.19}$
120–200	152	$2.87^{+0.53}_{-0.45}$	$0.88^{+0.33}_{-0.25}$	31^{+12}_{-10}	$1.84^{+0.44}_{-0.36}$	64^{+18}_{-17}	$1.19^{+0.37}_{-0.29}$	$0.65^{+0.30}_{-0.21}$
200–500	306	$4.02^{+0.74}_{-0.63}$	$1.30^{+0.47}_{-0.36}$	32^{+13}_{-11}	$2.61^{+0.62}_{-0.51}$	65^{+18}_{-17}	$2.11^{+0.57}_{-0.46}$	$0.51^{+0.34}_{-0.22}$
500–2000	1032	$6.71^{+1.86}_{-1.49}$	$0.67^{+0.88}_{-0.43}$	10^{+13}_{-7}	$5.70^{+1.74}_{-1.37}$	85^{+32}_{-31}	$5.37^{+1.70}_{-1.33}$	$0.34^{+0.77}_{-0.28}$
2000–100000	17262	$42.4^{+12.5}_{-9.9}$	...	...	$42.4^{+12.5}_{-9.9}$	100^{+38}_{-38}	$42.4^{+12.5}_{-9.9}$	...

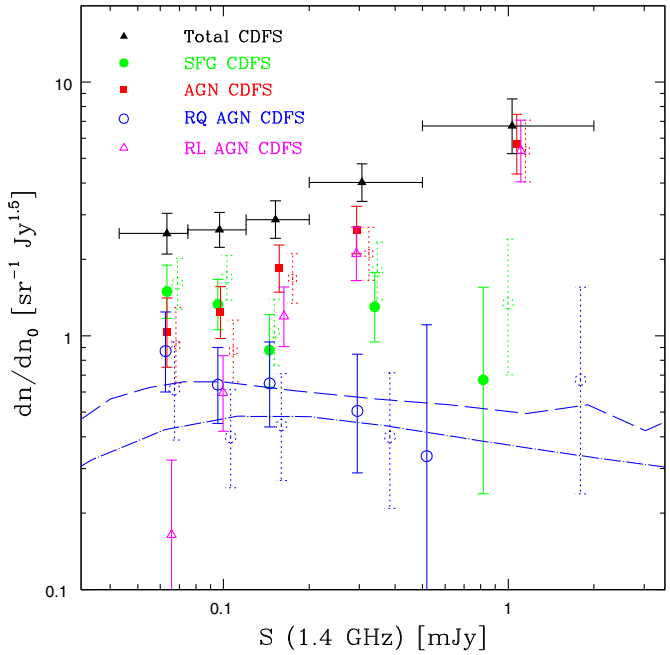

Figure 4. Euclidean normalized 1.4 GHz CDFS source counts: total counts (black triangles), SFGs (filled green circles), all AGNs (red squares), radio-quiet AGNs (open blue circles), and radio-loud AGNs (open magenta triangles). Error bars correspond to 1σ errors (Gehrels 1986). The dotted symbols are the source counts from Paper IV (shifted by 0.035 dex for clarity). The long-dashed and dot-dashed lines are the radio-quiet AGN number counts predicted by Wilman et al. (2008) and Padovani et al. (2009), respectively, based on X-ray data. See the text for details.

(A color version of this figure is available in the online journal.)

values. Coupled with a $q > 1.7$ it would then be classified as an SFG but its location on the IRAC color–color plot puts it firmly with the radio-quiet AGN. NGC 1052, an elliptical galaxy often classified as a low-ionization nuclear emission-line region (LINER), also has low R, P_r, and $L_x(2–10\,keV)$ values but its low q makes it a radio-loud AGN. M 82, the prototype starburst galaxy, again has low R, P_r, and $L_x(2–10\,keV)$ values but its $q > 1.7$ and location on the IRAC diagram classify it as an SFG. And NGC 1275, a cD (radio) galaxy at the center of the Perseus cluster, which in the literature has been classified, among other things, as a Seyfert 1.5 galaxy and a blazar, with its high R, P_r, and very low q, is undoubtedly a radio-loud AGN.

Table 1 and Figure 4 present the Euclidean normalized number counts for the revised sample, compared to those from Paper IV shown in the figure. As expected from the revised classification, SFGs show a small decrease, while AGNs and radio-quiet AGNs increase slightly in number. However, the revised number counts are still within 1σ from the old ones, and most of the largest changes happen at higher flux densities. Note that SFGs are still predominant below ~0.1 mJy, which is also the flux density at which radio-quiet AGNs start to outnumber radio-loud ones.

AGNs make up 49^{+7}_{-6}% (where the errors are based on binomial statistics: Gehrels 1986) of sub-millijansky sources and their counts are seen to drop at lower flux densities, going from 100% of the total at ~10 mJy down to 41% at the survey limit. SFGs, on the other hand, which represent 50^{+8}_{-7}% of the sample, are missing at high flux densities but become the dominant population below ≈0.1 mJy, reaching 59% at the survey limit. Radio-quiet AGNs represent 28^{+6}_{-5}% (or 57% of all AGNs) of sub-millijansky sources but their fraction appears to increase at lower flux densities, where they make up 84% of all AGNs and ≈34% of all sources at the survey limit, up from ≈5% at ≈1 mJy.

Middelberg et al. (2011) have recently detected with the Very Long Baseline Array (VLBA) 20 VLA-CDFS sources using a resolution of ~0.″025. With a limit of ~0.5 mJy, Very Long Baseline Interferometry (VLBI) detections above $z > 0.1$ are most likely to be due to AGNs. Reassuringly, all of the 20 detected VLBA objects (which have $z > 0.15$) were classified as radio-loud AGNs by our method.

Figure 5 shows radio power versus redshift for our sources, with the dotted lines indicating 43 μJy, the faintest radio flux density of our sample (lower line), and 100 μJy (upper line: see Section 3) for $\alpha_r = 0.7$.

3. EVOLUTION

3.1. V_e/V_a Analysis

We first study the evolutionary properties of the VLA-CDFS sample through a variation of the V/V_{max} test (Schmidt 1968)—the V_e/V_a test (Avni & Bahcall 1980; Morris et al. 1991), that is, the ratio between *enclosed* and *available* volume. This is because we do not have a single flux limit but the sensitivity of our sample is a function of the position in the field of view (see Paper I) and, consequently, the area of the sky covered at any given flux density (usually known as the sky coverage) is flux dependent. This ranges from a maximum of 0.2 deg^2 for radio flux densities ⩾295 mJy, to 0.14 deg^2 at 100 mJy, down to 0.01 deg^2 at the flux density limit.

Values of $\langle V_e/V_a \rangle$ significantly different from 0.5 and a distribution significantly different from uniform indicate evolution, which is positive (sources were more luminous and/or more numerous in the past) when $\langle V_e/V_a \rangle > 0.5$, and negative (sources were less luminous and/or less numerous in the past) when <0.5. Moreover, one can also fit an evolutionary model to

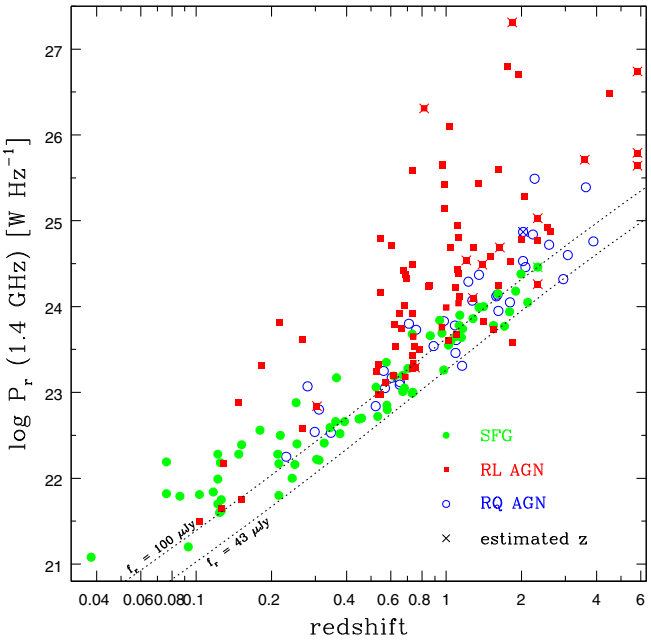

Figure 5. Radio power vs. redshift for our sample. Filled circles indicate SFGs, filled squares radio-loud AGNs, and open circles radio-quiet AGNs. Crosses denote redshifts estimated from the optical magnitude. The power–redshift relationships for a flux density of 43 μJy (lower dotted line) and 100 μJy (upper dotted line) assuming a radio spectral index of 0.7 are also shown.

(A color version of this figure is available in the online journal.)

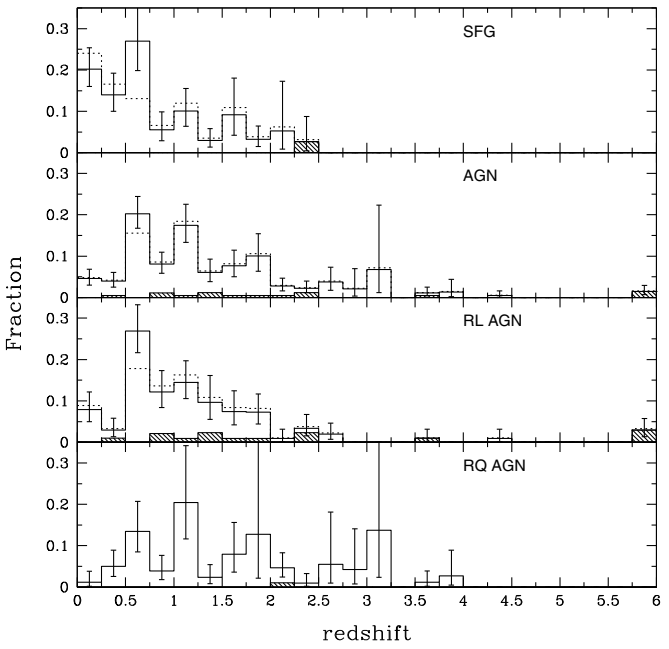

Figure 6. Fractional redshift distributions for the different classes of sources, deconvolved with the appropriate sky coverage. The dashed areas denote redshifts estimated from the optical magnitude. Error bars represent the 1σ range based on Poisson statistics. The dotted lines exclude all sources in the two large-scale concentrations at $0.664 \leqslant z \leqslant 0.685$ and $0.725 \leqslant z \leqslant 0.742$ (Gilli et al. 2003).

the sample by finding the evolutionary parameter which makes $\langle V_e/V_a\rangle = 0.5$. Note that the V_e/V_a test is independent of the shape of the LF, unlike the maximum likelihood method used below.

We have computed V_e/V_a values for our sources taking into account the appropriate sky coverage (see Equations (42) and (43) of Avni & Bahcall 1980), k-correcting the radio powers as described in Section 2.3. Statistical errors are given by $\sigma = 1/\sqrt{12N}$ (Avni & Bahcall 1980). We estimate the significance of the deviation from the non-evolutionary case by assessing the probability P_{ev} that the V_e/V_a distribution is different from uniform according to a Kolmogorov–Smirnov (K-S) test. Similar results are obtained by using the deviation from 0.5 of $\langle V_e/V_a\rangle$. To have a simple estimate of the sample evolution we have also derived the best-fit parameter k_L assuming a pure luminosity evolution (PLE) of the type $P(z) = P(0)(1+z)^{k_L}$ or a pure density evolution (PDE) of the type $\Phi(z) = \Phi(0)(1+z)^{k_D}$, where $\Phi(z)$ is the LF.

We assume that some luminosity evolution takes place, based on previous studies in the radio and other bands. When the best fit indicates negative luminosity evolution (i.e., $k_L < 0$), however, we fit a pure density evolution model as well, which we feel is more physical in this case. Note that for a single power-law LF $\Phi(P) \propto P^{-\gamma}$ the evolutionary parameters in the two cases are related through the simple relationship $k_D = k_L(\gamma - 1)$ (e.g., Marshall et al. 1983).

Our results are shown in Table 2, which gives the sample in column (1), the number of sources in column (2), the mean redshift in column (3), the percentage of sources with redshift estimated from the magnitude in column (4), $\langle V_e/V_a\rangle$ in column (5), the probability P_{ev} that the V_e/V_a distribution is different from uniform in column (6), and the best-fit parameters k_L and k_D (when applicable) in columns (7) and (8), respectively (only when $P_{ev} > 95\%$). The mean redshift is calculated taking into account the effect of the sky coverage, that is, each object is weighted by the inverse of the area accessible at the flux density of the source (see, e.g., Padovani et al. 2007).

The fractional redshift distributions for the different classes are shown in Figure 6. As also shown in Table 2, radio-quiet AGNs have the highest $\langle z\rangle$ and reach $z \sim 3.9$. Radio-loud AGNs have the broadest distribution, extending up to $z \sim 6$ but with a lower $\langle z\rangle$ than radio-quiet ones. SFGs despite the relatively narrow redshift range ($z \leqslant 2.3$) have a $\langle z\rangle$ not too different from that of radio-loud AGNs and much smaller than radio-quiet ones. Most classes show strong peaks at $z \sim 0.5 - 0.75$. These are related for all classes apart from radio-quiet AGNs to the two large-scale structures detected in the CDFS by Gilli et al. (2003) in the $0.664 \leqslant z \leqslant 0.685$ and $0.725 \leqslant z \leqslant 0.742$ ranges, which, as shown in the figure, contribute substantially to the observed peaks. The effect of these structures on our results is discussed in Section 5.2.

The main results on the sample evolution are the following.

1. The whole sample has $\langle V_e/V_a\rangle > 0.5$ and shows a significant departure from the non-evolutionary case ($P_{ev} \sim 99\%$) with an evolution characterized by $k_L = 0.9^{+0.3}_{-0.4}$.
2. SFGs evolve at a very high significance level ($P_{ev} > 99.9\%$); their evolutionary parameter for the case of pure luminosity evolution is $k_L = 2.5^{+0.2}_{-0.3}$.
3. AGNs as a whole do not appear to evolve, as their $\langle V_e/V_a\rangle$ is only slightly below 0.5 (by $\sim 0.8\sigma$) and the V_e/V_a distribution is not significantly different from uniform ($P_{ev} \sim 66\%$).
4. Radio-quiet AGNs, however, evolve very significantly ($P_{ev} > 99.9\%$) with $k_L = 2.5^{+0.2}_{-0.3}$, the same value as that of SFGs.
5. Radio-loud AGNs also evolve significantly ($P_{ev} = 99.5\%$) but in a negative sense, with $k_L = -3.0^{+1.0}_{-1.1}$ or $k_D = -1.6\pm 0.4$. However, this is largely due to the high power sources. Figure 7 shows that V_e/V_a values are strongly dependent on

Table 2
Sample Evolutionary Properties: V_e/V_a Analysis

Sample	N	$\langle z\rangle$	Estimated z %	$\langle V_e/V_a\rangle$	P_{ev}	k_L[a]	k_D[b]
All sources	193	1.18 ± 0.07	8.3%	0.544 ± 0.021	98.8%	$0.9^{+0.3}_{-0.4}$	...
SFGs	71	0.90 ± 0.07	1.4%	0.655 ± 0.034	>99.9	$2.5^{+0.2}_{-0.3}$	...
All AGNs	122	1.44 ± 0.09	12.3%	0.479 ± 0.026	65.6%	[c]	[c]
Radio-quiet AGNs	36	1.73 ± 0.16	2.8%	0.727 ± 0.048	>99.9	$2.5^{+0.2}_{-0.3}$	...
Radio-loud AGNs	86	1.26 ± 0.11	16.3%	0.375 ± 0.031	99.5%	$-3.0^{+1.0}_{-1.1}$	-1.6 ± 0.4
Radio-loud AGNs, $P < 10^{24.5}$ W Hz^{-1}	53	0.84 ± 0.06	9.4%	0.432 ± 0.040	76.2%	[c]	[c]
Radio-loud AGNs, $P > 10^{24.5}$ W Hz^{-1}	33	2.01 ± 0.26	27.3%	0.285 ± 0.050	99.9%	...	$-1.8^{+0.8}_{-0.9}$

Notes.
[a] Pure luminosity evolution $P(z) = P(0)(1+z)^{k_L}$.
[b] Pure density evolution $\Phi(z) = \Phi(0)(1+z)^{k_D}$.
[c] $P_{ev} < 95\%$: no evolution required.

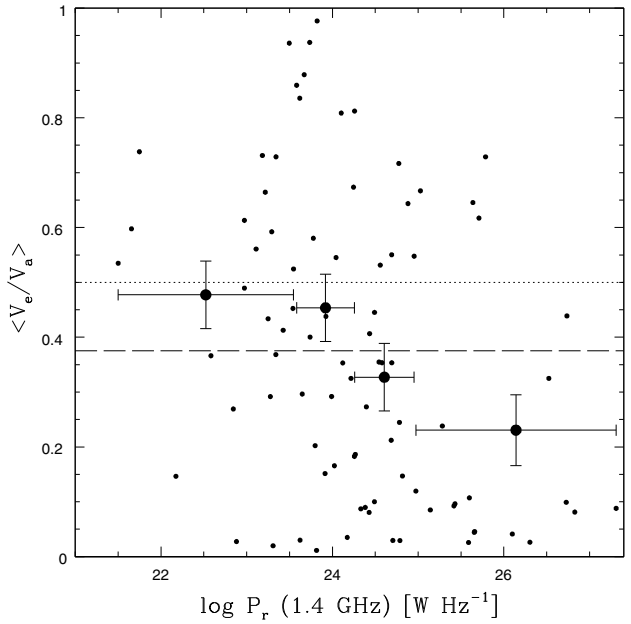

Figure 7. V_e/V_a values and means vs. radio power for radio-loud AGNs. The dashed line indicates the mean value for the whole sample, while the dotted line is the non-evolutionary value (0.5). Vertical error bars represent the 1σ range based on Poisson statistics while the horizontal ones give the covered range of powers.

radio power, with $\langle V_e/V_a\rangle$ becoming significantly ($\sim 2.8\sigma$) smaller than 0.5 for $P > 2 \times 10^{24}$ W Hz^{-1}. We then split the radio-loud AGN sample at $P = 10^{24.5}$ W Hz^{-1}. The low-power subsample does not appear to evolve, as its $\langle V_e/V_a\rangle$ is not significant ($\sim 1.7\sigma$) < 0.5 and its V_e/V_a distribution is not significantly different from uniform ($P_{ev} \sim 76\%$). On the other hand, the high-power subsample anti-evolves at a very high significance level ($P_{ev} \sim 99.9\%$), with $k_D = -1.8^{+0.8}_{-0.9}$. Because of the luminosity difference, the two subsamples also have very different redshift distributions, with $\langle z\rangle \sim 0.8$ (range: $\sim$0.1–2.3) and 2.0 (range: $\sim$0.5–5.8), respectively. This also means that the low-redshift evolution of the high-power sub-class is not well determined since, for example, only eight such sources (24%) have $z \leqslant 1$ (see Section 4).

3.2. Maximum Likelihood Analysis

A more general approach to estimate the evolution, and at the same time the LF, is to perform a maximum likelihood fit of an evolving luminosity function to the observed distribution in luminosity and redshift. This approach makes maximal use of the data and is free from arbitrary binning; however, unlike the V_e/V_a test, it is model dependent. We follow the prescription of Marshall et al. (1983) and minimize the following quantity:

$$S = -2\sum_{i}^{N} \ln[\Phi(P_i, z_i)] + 2\int_{P_{min}}^{P_{max}}\int_{z_{min}}^{z_{max}} \Phi(P,z)\Omega(f(P,z))\frac{dV}{dz}dz\,dP, \quad (3)$$

where $\Phi(P,z)$ is the luminosity function, $\Omega(f)$ is the sky coverage, and dV is the differential comoving volume. The sum is extended over the whole sample, while the double integral is computed over the luminosity range appropriate for the adopted evolution and over the observed redshift range (see Marshall et al. 1983 for more details). The best-fit parameters are determined by minimizing S and their associated errors are computed by varying the parameter of interest until an increment ΔS over the minimum value is obtained. 1σ errors for one parameter correspond to $\Delta S = 1.0$ while confidence contours for 1, 2, and 3σ levels for two interesting parameters are derived for $\Delta S = 2.3$, 6.17, and 11.8, respectively (Press et al. 1986). We consider one and two power-law LFs, that is, $\Phi(P) \propto P^{-\gamma_2}$ and $\Phi(P) \propto 1/[(P/P_*)^{\gamma_1} + (P/P_*)^{\gamma_2}]$, respectively.

Our results are shown in Table 3, which gives the sample in column (1), the evolutionary model in column (2), the two slopes (if applicable) of the LF in columns (3) and (4), the best-fit evolutionary parameter in column (5), and the break power (if applicable) in column (6). Errors are 1σ for one interesting parameter. The best-fit evolutionary parameters agree extremely well (mostly within 1σ) with those derived through the V_e/V_a approach.

4. LUMINOSITY FUNCTIONS

Figure 8 shows that, assuming a single power-law LF and applying the maximum likelihood method, SFGs and AGNs, when considered as a single class, have widely different forms of evolution, as seen above, but also different LF slopes, with $\Phi(P) \propto P^{-2.6}$ and $\Phi(P) \propto P^{-1.6}$, respectively. The 3σ confidence contours have no overlap. The situation is even more extreme when one compares SFGs with radio-loud AGNs. On the contrary, in the case of the radio-quiet AGN the best-fit parameters are the same as SFGs (within less than 1σ) and the

Table 3
Sample Luminosity Functions and Evolution: Maximum Likelihood Analysis

Sample	Model	γ_1	γ_2	k	$\log P_*$ (W Hz^{-1})
SFGs	PLE	...	2.56 ± 0.09	$2.87^{+0.06}_{-0.21}$	...
SFGs	PLE	$1.3^{+0.5}_{-0.9}$	$3.15^{+0.38}_{-0.27}$	$2.89^{+0.10}_{-0.15}$	$21.85^{+0.22}_{-0.27}$
All AGNs	PLE	...	1.60 ± 0.05	-1.5 ± 0.6	...
Radio-quiet AGNs	PLE	...	2.6 ± 0.3	$2.5^{+0.4}_{-0.5}$	...
Radio-loud AGNs	PLE	...	1.46 ± 0.06	$-3.7^{+1.1}_{-1.6}$	...
Radio-loud AGNs	PDE	...	1.45 ± 0.06	-1.8 ± 0.4	...
Radio-loud AGNs, $P < 10^{24.5}$ W Hz^{-1}	PDE	...	$1.42^{+0.14}_{-0.12}$	$-1.5^{+0.9}_{-0.8}$	...
Radio-loud AGNs, $P > 10^{24.5}$ W Hz^{-1}	PDE	...	1.46 ± 0.12	-1.8 ± 0.6	...

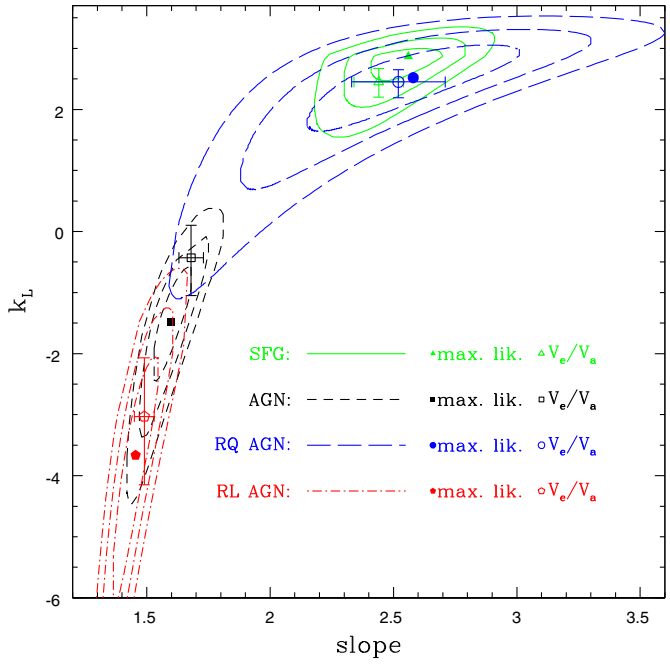

Figure 8. Maximum likelihood confidence contours (1σ, 2σ, and 3σ) for the evolutionary parameter k_L and the single power-law slope of the LF. The best-fit values for the various classes are indicated by the various symbols, with the filled ones referring to the maximum likelihood analysis and the open ones pertaining to the V_e/V_a approach. Note that the slope of the LF in the latter case depends on the adopted bin size in logarithmic power and is therefore only indicative.

(A color version of this figure is available in the online journal.)

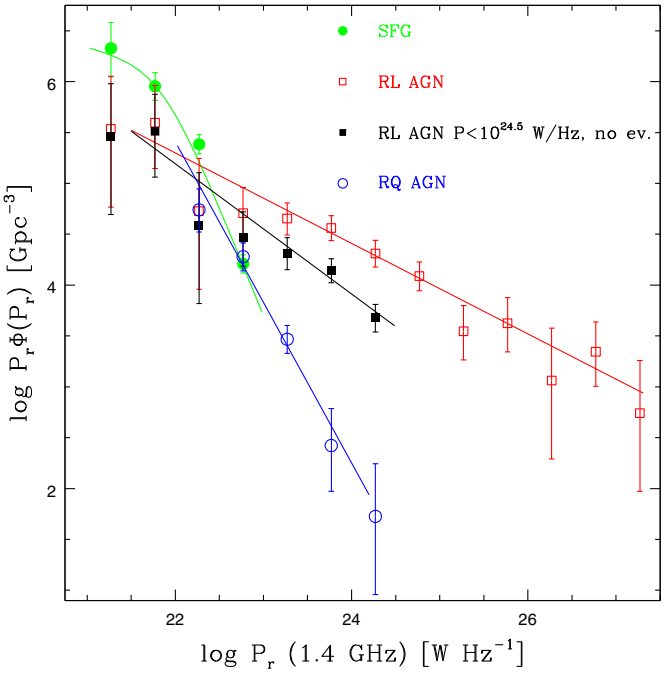

Figure 9. Local differential 1.4 GHz LFs for SFGs and AGNs in a $P \times \phi(P)$ form obtained with the maximum likelihood method (solid lines) and the LFs de-evolved to $z = 0$ using the best-fit evolutionary parameters from the maximum likelihood analysis (points). Filled circles indicate SFGs, open squares radio-loud AGNs, filled squares radio-loud AGNs with $P < 10^{24.5}$ W Hz^{-1}, and open circles radio-quiet AGNs. The LFs for radio-loud AGNs with $P < 10^{24.5}$ W Hz^{-1} from both methods are shown without any de-evolution as inferred from the $\langle V_e/V_a \rangle$ analysis. Error bars correspond to 1σ Poisson errors (Gehrels 1986) evaluated using the number of sources per bin with redshift determination only. See the text for details.

(A color version of this figure is available in the online journal.)

confidence contours overlap to a large extent (although the radio-quiet AGN contours are wider due to their smaller number). Finally, radio-quiet and radio-loud AGNs have very different LFs and evolution parameters, with only a tiny overlap of the 3σ confidence contours and the former having a much steeper LF than the latter ($\Phi(P) \propto P^{-2.6}$ versus $\Phi(P) \propto P^{-1.45}$).

The shape of the SFG LF is more complex than for the other classes, as the maximum likelihood double power-law fit, given in Table 3, excludes the case $\gamma_1 = \gamma_2$ with a significance well above 3σ, which implies that a single power law is not a good representation of the data. The best fit has $\Phi(P) \propto P^{-1.3}$ and $\Phi(P) \propto P^{-3.15}$ at the faint and bright ends, respectively, with a break at $P \sim 7 \times 10^{21}$ W Hz^{-1}.

Figure 9 shows the local LFs derived from the maximum likelihood best fits compared with those obtained from the $1/V_{max}$ (in our case $1/V_a$) technique without any assumption on the LF but de-evolved to $z = 0$ using the best-fit evolutionary parameters. The LFs are shown in a $P \times \Phi(P)$ form, which is almost equivalent[7] to the $\phi(M_B)$ form normally used in the optical band and allows an easy separation of luminosity and density evolution as the former would simply translate the LF to the right (higher powers) with no change in the ordinate (number), while the opposite would be true for the latter.

The maximum likelihood fits, although relatively simple, appear to be very good representations of the LFs obtained with the $1/V_a$ technique. From Figure 9 one also infers that AGNs dominate over SFGs for $P \gtrsim 3 \times 10^{22}$ W Hz^{-1}, in agreement

[7] $P \times \Phi(P) = 2.5/ln(10) \times \Phi(M) \sim 1.09 \times \Phi(M)$, where the units of $\Phi(M)$ are mag^{-1} Volume^{-1}. Note that these units are also sometimes used in the radio band; see, e.g., Condon (1989); Sadler et al. (2002); Mauch & Sadler (2007).

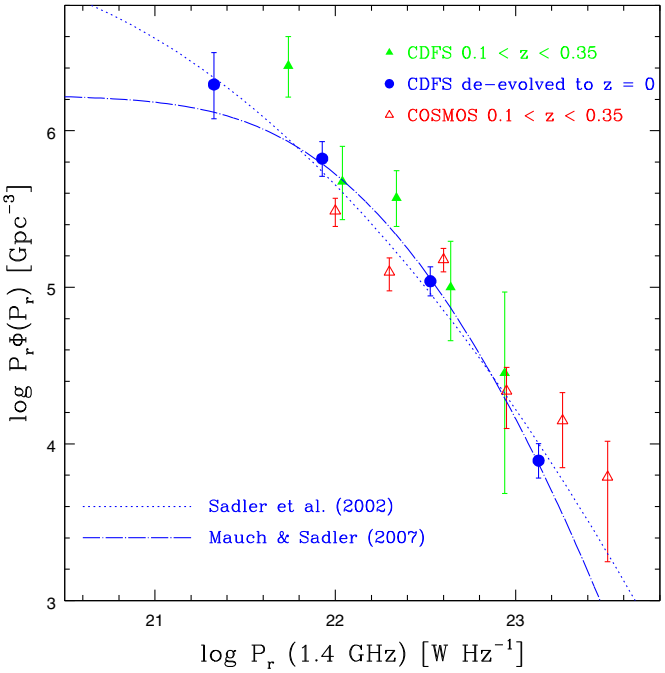

Figure 10. Local differential 1.4 GHz LF for SFGs in a $P \times \phi(P)$ form. Filled triangles indicate the VLA-CDFS LF in the 0.1–0.35 redshift range, open triangles refer to the COSMOS LF in the same range, and filled circles denote the LF de-evolved to $z = 0$ using the best-fit evolutionary parameter from the $\langle V_e/V_a \rangle$ analysis. The best fits to the local SFG LF from Sadler et al. (2002; converted to our value of H_0) and Mauch & Sadler (2007) are also shown (dotted and dash-dotted lines, respectively). Error bars correspond to 1σ Poisson errors (Gehrels 1986) evaluated using the number of sources per bin with redshift determination only. See the text for details.

(A color version of this figure is available in the online journal.)

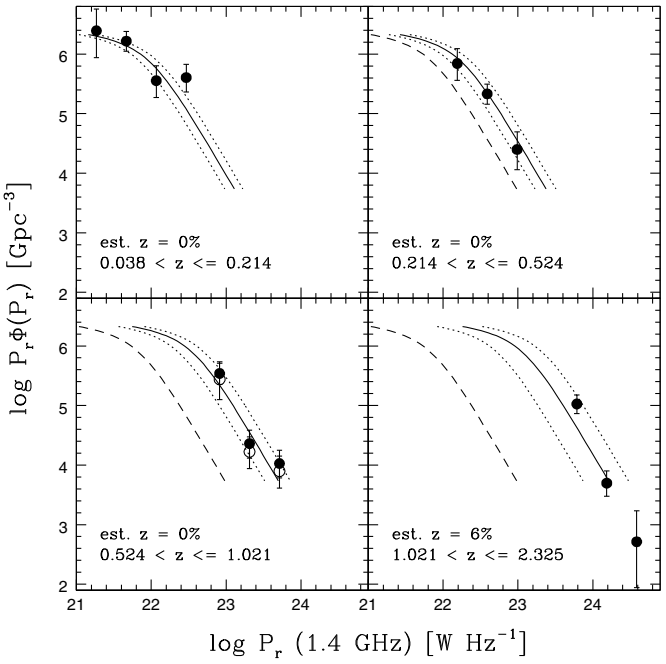

Figure 11. Differential 1.4 GHz LF for VLA-CDFS SFGs in a $P \times \phi(P)$ form in four redshift bins. The solid lines represent the best-fit double power-law LF from the maximum likelihood method evolved to the central redshift of the bin using the best-fit evolution $(1+z)^{2.89}$, with dotted lines showing the same LF at the two extreme redshifts defining the bin. The short-dashed line represents the LF at $z = 0$. Error bars correspond to 1σ Poisson errors (Gehrels 1986) evaluated using the number of sources per bin with redshift determination only. The percentage of redshifts estimated from the optical magnitude is also given for each bin. Open symbols in the 0.524–1.021 bin do not include the seven sources in the two large-scale concentrations at $0.664 \leqslant z \leqslant 0.685$ and $0.725 \leqslant z \leqslant 0.742$ (Gilli et al. 2003). See the text for details.

with previous studies (e.g., Mauch & Sadler 2007). Moreover, radio-loud AGNs have a much flatter LF than radio-quiet ones and are predominant at $P \gtrsim 6 \times 10^{22}$ W Hz^{-1}. Finally, the radio-quiet AGN LF seems to be an extension of the SFG one at higher radio powers.

It is important to be aware of the fact that the low-redshift behavior of the high-power radio-loud AGN is not well determined. Based on previous results (see Section 5.5.2) we would in fact expect a strong positive evolution at moderately low redshifts followed by a decline at higher redshifts. Our sample is too small to detect such a change, since it is dominated by high-redshift objects (∼3/4 of the sample has $z > 1$). This means that the best-fit PDE largely reflects the high-redshift negative evolution and, once the LF is de-evolved to $z = 0$, this translates into an artificially large density of sources at high powers. We therefore also plot in Figure 9 the LF of $P < 10^{24.5}$ W Hz^{-1} sources with their evolution fixed to zero, based on the results of the $\langle V_e/V_a \rangle$ analysis, which should give a more realistic estimate of the local LF.

We now concentrate on the details of the individual classes.

4.1. SFGs

Figure 10 shows different estimates of the local LF for our SFGs. Filled triangles indicate the VLA-CDFS SFG LF in the 0.1–0.35 redshift range, to compare it with the COSMOS LF (Smolčić et al. 2009a) in the same range (open triangles). The two LFs are within 1σ apart from one bin. Our LF is "noisier" as we only have 24 objects in this redshift bin, compared with 98 for the COSMOS sample. We also note that the selection criteria of the two samples are very different, with the COSMOS one being based on a rest-frame optical color classification (Smolčić et al. 2008).

To have a more robust estimate of the local LF for SFGs we have derived the LF de-evolved to $z = 0$ (filled circles) using the best-fit evolutionary parameter from the $\langle V_e/V_a \rangle$ analysis. This makes use of the whole sample but is obviously dependent on the assumed evolutionary model. In Figure 10 we also plot the best fits to the local ($z \leqslant 0.3$) LFs from Sadler et al. (2002) and Mauch & Sadler (2007) (dotted and dash-dotted lines, respectively). Both our local LFs are consistent with these two LFs, particularly the de-evolved one ($\chi^2_\nu < 0.6$). This validates our selection method. As was the case for the maximum likelihood approach, a single power-law fit is inconsistent with the de-evolved local LF ($\chi^2_\nu \sim 3.4$, significant at the ∼97% level).

The maximum likelihood fit provides a very good representation of the redshift evolution of the LF of SFGs, as shown in Figure 11 (tabulated in Table 4), which plots the SFG LF over the full redshift range sampled, that is, 0–2.3, in four redshift bins each containing a similar number of objects. The median enclosed volumes for the four bins are 3×10^{-6}, 2×10^{-5}, 9×10^{-5}, and 5×10^{-4} Gpc^3, respectively.

4.2. AGNs

Figure 12 shows different estimates of the local LF for our AGNs. Filled triangles indicate the VLA-CDFS AGN LF in the 0.1–0.35 redshift range, to compare it with the COSMOS LF (Smolčić et al. 2009b) in the same range (open triangles). The two LFs are within $\approx 1\sigma$. As was the case for SFGs, our LF is

Table 4
Luminosity Functions for VLA-CDFS Star-forming Galaxies

Redshift Range	$\log P_{1.4\mathrm{GHz}}$ (W Hz^{-1})	$\log P\Phi(P)$ (Gpc^{-3})	N
$0.038 < z \leqslant 0.214$	21.27	$6.39^{+0.36}_{-0.45}$	2
	21.67	$6.22^{+0.16}_{-0.17}$	9
	22.07	$5.55^{+0.25}_{-0.28}$	4
	22.47	$5.61^{+0.22}_{-0.24}$	5
$0.214 < z \leqslant 0.524$	22.19	$5.84^{+0.25}_{-0.28}$	4
	22.59	$5.33^{+0.16}_{-0.17}$	9
	22.99	$4.40^{+0.29}_{-0.34}$	3
$0.524 < z \leqslant 1.021$	22.91	$5.54^{+0.17}_{-0.18}$ ($5.44^{+0.29}_{-0.34}$)	8 (3)
	23.31	$4.36^{+0.22}_{-0.24}$ ($4.22^{+0.25}_{-0.28}$)	5 (4)
	23.71	$4.03^{+0.22}_{-0.24}$ ($3.90^{+0.25}_{-0.28}$)	5 (4)
$1.021 < z \leqslant 2.325$	23.79	$5.03^{+0.15}_{-0.16}$	10
	24.19	$3.70^{+0.20}_{-0.22}$	6
	24.59	$2.71^{+0.52}_{-0.77}$	1

Notes. Numbers in parenthesis exclude the seven sources in the two large-scale concentrations at $0.664 \leqslant z \leqslant 0.685$ and $0.725 \leqslant z \leqslant 0.742$ (Gilli et al. 2003). Errors correspond to 1σ Poisson errors (Gehrels 1986) evaluated using the number of sources per bin with redshift determination only. The conversion to units of Mpc^{-3} dex^{-1} used, for example, by Smolčić et al. (2009a), is done by subtracting $9 - \log(\ln(10))$ from our values.

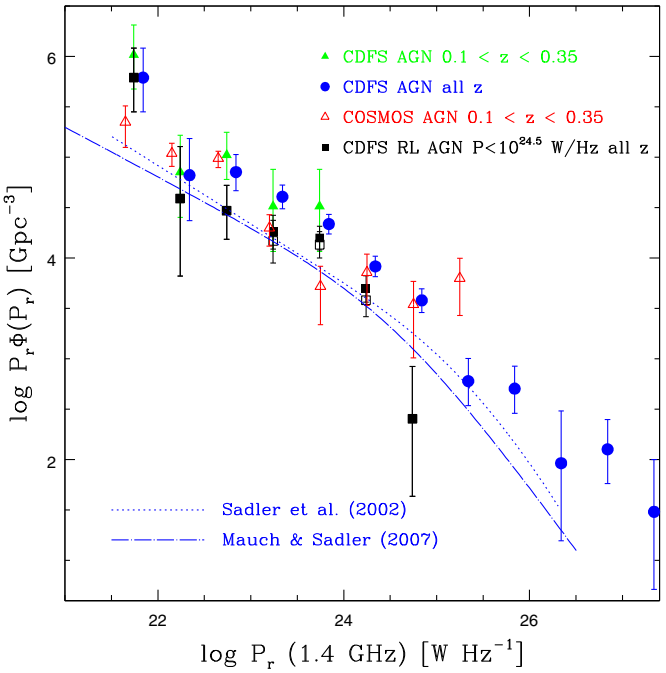

Figure 12. Local differential 1.4 GHz LF for AGNs in a $P \times \phi(P)$ form. Filled triangles indicate the VLA-CDFS LF in the 0.1–0.35 redshift range, open triangles refer to the COSMOS LF in the same range, filled circles denote the full AGN LF (shifted by 0.1 in log P for clarity), while filled squares are the radio-loud AGNs with $P < 10^{24.5}$ W Hz^{-1} (with open squares showing the effect of excluding the 10 sources in the two large-scale concentrations at $0.664 \leqslant z \leqslant 0.685$ and $0.725 \leqslant z \leqslant 0.742$; Gilli et al. 2003). Both of these LFs are shown without any de-evolution as inferred from the $\langle V_e/V_a \rangle$ analysis. The best fits to the local AGN LF from Sadler et al. (2002) (converted to our value of H_0) and Mauch & Sadler (2007) are also shown (dotted and dash-dotted lines, respectively). Error bars correspond to 1σ Poisson errors (Gehrels 1986) evaluated using the number of sources per bin with redshift determination only. See the text for details.

(A color version of this figure is available in the online journal.)

"noisier" as we only have 15 objects in this redshift bin. The selection criteria for the two samples are also quite different and quasars ($\lesssim$20% of the AGN sample) were not included by Smolčić et al. (2009b). We also show the full LF for all AGNs (filled circles) assuming no evolution, as inferred from our analysis.

In Figure 12 we also plot the best fits to the local ($z \leqslant 0.3$) LFs from Sadler et al. (2002) and Mauch & Sadler (2007) (dotted and dash-dotted lines, respectively). Both of our LFs are inconsistent with these previous estimates ($\chi^2_\nu \geqslant 3.0$, significant at the >98.9% level) and a factor of $\sim$ 2–4 higher. This is also true of the COSMOS LF of Smolčić et al. (2009b) ($\chi^2_\nu \sim 4.6$, significant at the >99.9% level), despite their claims to the contrary. Two effects are at play here. The first, and more important one, is that the AGN LF includes a sizable contribution from radio-quiet AGNs, which were not present in significant numbers in previous LFs as these were based on the NRAO VLA Sky Survey ($S_{\mathrm{min}} \gtrsim 2.8$ mJy), while radio-quiet AGNs make up a non-negligible fraction of radio sources only below $\approx$1 mJy (Figure 4), and both included only non-stellar optical sources. Note that none of these arguments apply to SFGs, which look non-stellar and, despite their relatively low fraction at high radio flux densities, were selected because of the low-redshift cuts (AGNs tend to have higher redshifts; see Figure 6) and, in the case of the Mauch & Sadler (2007) sample, the K-band selection. (This bias is vividly illustrated by Figure 5 of Mauch & Sadler 2007, where SFGs dominate below $\sim$10 mJy, while Figure 4 shows that in purely radio selected samples without any redshift cut this happens below $\sim$0.1 mJy.) If one considers only radio-loud AGNs with $P < 10^{24.5}$ W Hz^{-1} (filled squares), which are non-evolving, our LF is marginally consistent with that from Sadler et al. (2002) ($\chi^2_\nu \sim 2.0$, significant at the $\sim$95% level). The second effect is related to cosmic variance: the exclusion of the 11 sources in the two large-scale concentrations at $0.664 \leqslant z \leqslant 0.685$ and $0.725 \leqslant z \leqslant 0.742$ (Gilli et al. 2003) (open squares), in fact, reduces even further the discrepancy with both previously determined local LFs, which are now consistent with ours ($\chi^2_\nu \leqslant 1.8$, significant at the $\leqslant$ 91% level).

The maximum likelihood best fits for the two classes of radio-loud AGNs, below and above $P = 10^{24.5}$ W Hz^{-1}, provide a good representation of the evolution and LF of radio-loud AGNs, as shown in Figure 13 (tabulated in Table 5), which plots the radio-loud AGN LF over the full redshift range sampled, that is, 0.1–5.8, in four redshift bins each containing a similar number of objects. (For the radio-loud AGN with powers below $10^{24.5}$ W Hz^{-1} we fixed the evolution to zero, based on the results of the V_e/V_a analysis, excluded the sources in the two large-scale redshift concentrations, and obtained $\Phi(P) \propto P^{-1.7\pm0.1}$.) The median enclosed volumes for the four bins are 2×10^{-4}, 7×10^{-5}, 2×10^{-4} and 10^{-3} Gpc^3, respectively.

We note that the high-power end of the radio luminosity function is poorly sampled because of the relatively small volume covered by our small-area field. This, combined with the fact that $\sim$30% of the redshifts for our high-power radio-loud AGNs have been estimated from the optical magnitude, makes our results for the $P > 10^{24.5}$ W Hz^{-1} sub-class more uncertain than for the other classes. Moreover, as discussed above, their low-redshift evolution is not well determined (the two lowest redshift bins include two and four objects, respectively), which also means that the best-fit LF derived by the maximum likelihood method is artificially high at $z \lesssim 1$.

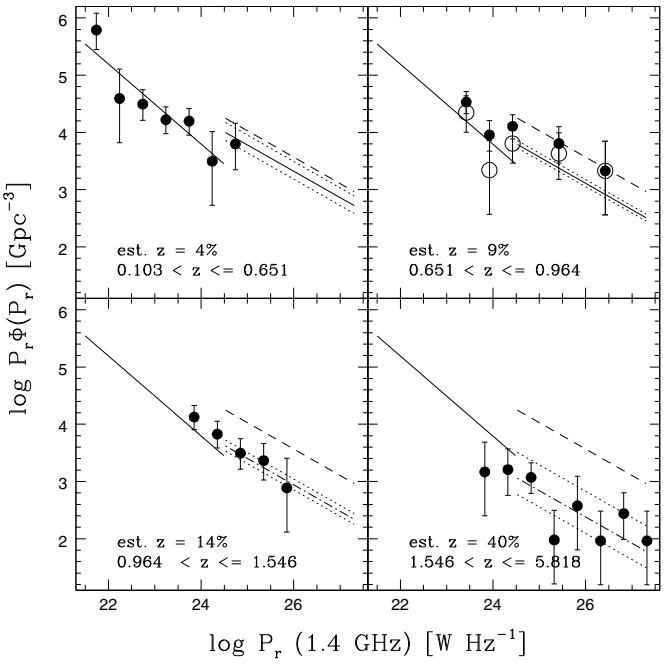

Figure 13. Differential 1.4 GHz LF for VLA-CDFS radio-loud AGNs in a $P \times \phi(P)$ form in four redshift bins. The solid lines represent the best-fit single power-law LF from the maximum likelihood method for $P < 10^{24.5}$ W Hz^{-1} (left) and $P > 10^{24.5}$ W Hz^{-1} (right), the latter evolved to the central redshift of the bin using the best fit for pure density evolution $(1+z)^{-1.8}$, with dotted lines showing the same LF at the two extreme redshifts defining the bin. The short-dashed line represents the best-fit LF at $z = 0$ for $P > 10^{24.5}$ W Hz^{-1}. Error bars correspond to 1σ Poisson errors (Gehrels 1986) evaluated using the number of sources per bin with redshift determination only. The percentage of redshifts estimated from the optical magnitude is also given for each bin. Open symbols in the 0.651–0.964 bin do not include the 11 sources in the two large-scale concentrations at $0.664 \leqslant z \leqslant 0.685$ and $0.725 \leqslant z \leqslant 0.742$ (Gilli et al. 2003). See the text for details.

Table 5
Luminosity Functions for VLA-CDFS Radio-loud AGNs

Redshift Range	$\log P_{1.4\,\mathrm{GHz}}$ (W Hz^{-1})	$\log P\Phi(P)$ (Gpc^{-3})	N
$0.103 < z \leqslant 0.651$	21.74	$5.79^{+0.29}_{-0.34}$	3
	22.24	$4.59^{+0.52}_{-0.77}$	1
	22.74	$4.49^{+0.25}_{-0.28}$	5
	23.24	$4.22^{+0.22}_{-0.24}$	5
	23.74	$4.20^{+0.22}_{-0.24}$	5
	24.24	$3.50^{+0.52}_{-0.77}$	1
	24.74	$3.80^{+0.36}_{-0.45}$	2
$0.651 < z \leqslant 0.964$	23.42	$4.53^{+0.19}_{-0.20}$ ($4.35^{+0.29}_{-0.34}$)	8 (4)
	23.92	$3.96^{+0.25}_{-0.28}$ ($3.34^{+0.52}_{-0.77}$)	4 (1)
	24.42	$4.11^{+0.20}_{-0.22}$ ($3.81^{+0.29}_{-0.34}$)	6 (3)
	25.42	$3.81^{+0.29}_{-0.34}$ ($3.63^{+0.36}_{-0.45}$)	3 (2)
	26.42	$3.33^{+0.52}_{-0.77}$ ($3.33^{+0.52}_{-0.77}$)	1 (1)
$0.964 < z \leqslant 1.546$	23.85	$4.13^{+0.20}_{-0.22}$	6
	24.35	$3.83^{+0.22}_{-0.24}$	8
	24.85	$3.49^{+0.25}_{-0.28}$	4
	25.35	$3.36^{+0.29}_{-0.34}$	3
	25.85	$2.89^{+0.52}_{-0.77}$	1
$1.546 < z \leqslant 5.818$	23.82	$3.17^{+0.52}_{-0.77}$	1
	24.32	$3.21^{+0.36}_{-0.45}$	3
	24.82	$3.07^{+0.25}_{-0.28}$	6
	25.32	$1.98^{+0.52}_{-0.77}$	1
	25.82	$2.58^{+0.52}_{-0.77}$	4
	26.32	$1.96^{+0.52}_{-0.77}$	1
	26.82	$2.44^{+0.36}_{-0.45}$	3
	27.32	$1.96^{+0.52}_{-0.77}$	1

Notes. Numbers in parenthesis exclude the 11 sources in the two large-scale concentrations at $0.664 \leqslant z \leqslant 0.685$ and $0.725 \leqslant z \leqslant 0.742$ (Gilli et al. 2003). Errors correspond to 1σ Poisson errors (Gehrels 1986) evaluated using the number of sources per bin with redshift determination only. The conversion to units of Mpc^{-3} dex^{-1} used, for example, by Smolčić et al. (2009b), is done by subtracting $9 - \log(\ln(10))$ from our values.

5. DISCUSSION

5.1. Effect of Missing Redshifts on Our Results

Since 14 out of 16 of the sources without redshift information are classified as radio-loud AGNs (mostly based on their q and R values), the other classes are basically unaffected by our redshift incompleteness. We checked how the redshifts estimated from the optical magnitude influence our results in two different ways. First, we assumed $z = \langle z \rangle = 1.13$ for these 16 sources. This is very different from our previous assumption, which resulted in a very broad redshift distribution extending between 0.3 and 5.8. The $\langle V_e/V_a \rangle$ (and best-fit evolutionary parameters) changed negligibly for all but one sub-class, at most by an amount equal to 0.4σ. Given the smaller redshifts (and therefore luminosity) involved, in fact, the sample of radio-loud AGNs with $P > 10^{24.5}$ W Hz^{-1} shrank by ∼18%, while their $\langle V_e/V_a \rangle$ decreased even further by 1.5σ reaching ∼0.21. Second, we estimated the missing redshifts using the scatter of the correlation between $\log z$ and V_{mag} (dashed lines in Figure 1). The anti-evolution of radio-loud AGNs was confirmed despite the substantial redshift variations ($P_{ev} > 97.2\%$), with changes in $\langle V_e/V_a \rangle$ only up to 0.6σ. In the case of high-power radio-loud AGNs the changes were somewhat larger, with an increase in $\langle V_e/V_a \rangle$ of 1.6σ when the upward scatter was applied (which however implies estimated redshifts up to ∼10). The evolution was nevertheless still strongly negative ($P_{ev} = 99\%$). As for low-power radio-loud AGNs, the changes in $\langle V_e/V_a \rangle$ were $<0.3\sigma$ with still no significant evidence for a departure from the non-evolutionary case ($P_{ev} < 86\%$).

In summary, our results are quite insensitive to the specific redshift values for the fraction of the sample without redshift information. This is not surprising, as redshift affects V_e/V_a values much less than flux density and our redshift incompleteness is very small (∼8%).

5.2. Effect of Large-scale Structures on Our Results

Gilli et al. (2003) studied the large-scale structure in the CDFS in the X-ray and near-IR bands and detected two concentrations of sources in the $0.664 \leqslant z \leqslant 0.685$ and $0.725 \leqslant z \leqslant 0.742$ ranges. Given the small area of our survey one could worry that such redshift spikes might influence some of our results. Indeed, the redshift distributions shown in Figure 6 peak in the 0.5–0.75 bin for most classes, but the peaks become much less pronounced when these objects are excluded. There are in fact 18 sources in these two redshift bins (7 SFGs and 11 AGNs), which make up ∼17% and ∼11% (taking into account the effect of the sky coverage) of all SFGs and radio-loud AGNs, respectively

(but 0% of radio-quiet AGNs and only ∼3% of high-power radio-loud AGNs).

To assess the *maximum* impact of these two structures on our results we studied the evolution of our sources by excluding *all* sources in these two redshift bins. The resulting $\langle V_e/V_a\rangle$ values and best-fit evolutionary parameters were within 1σ from those derived from the full samples for all classes, which shows that the effect of these large-scale structures on our results is minimal. These overdensities are obviously more noticeable when one studies the evolution of the LF with redshift (see, e.g., the bottom left panel of Figure 11 and the top right panel of Figure 13) but even then the revised LFs are within $\lesssim 1\sigma$ from the old ones. The exclusion of these sources has also some effect when we limit the SFG and radio-loud AGN samples to $z \leqslant 1.3$ (Section 5.6).

5.3. Are There Two Classes of Low Radio Power AGNs?

We have identified two classes of low-power AGNs: radio-quiet ones, defined as spelled out in Section 2, ∼94% of which turn out to have $P_r < 10^{25}$ W Hz^{-1}, and radio-loud ones, characterized by $P_r \lesssim 3 \times 10^{24}$ W Hz^{-1}. Both classes have also relatively low R values, as implicit in our selection of radio-quiet sources and as shown in Figure 3 of Padovani et al. (2009). One obvious question is, then, what the differences between these two classes are. The answer is: many. First, they have very different ($P > 99.99\%$) distributions in IRAC flux ratios (Section 2), according to a two-dimensional K-S test (Fasano & Franceschini 1987), with radio-loud AGNs mostly toward the old stellar population locus and the majority of radio-quiet AGNs populating the region where most unobscured AGNs should be (note that none of the selection requirements for the radio-loud/radio-quiet distinction were based on that). Second, despite the similar radio powers, they have very different redshift distributions ($P > 99.9\%$) and $\langle z\rangle$, 1.73 and 0.84 for radio-quiet and low-power radio-loud AGNs, respectively. Third, they evolve very differently and have different LFs, with radio-quiet AGNs characterized by a steep LF and strong positive evolution while low-power radio-loud AGNs display a much flatter LF and no evolution (and in any case $\langle V_e/V_a\rangle < 0.5$; see Section 3). Fourth, they have very different X-ray-to-radio luminosity distributions and ratios. To properly take into account the upper limits on X-ray power we used ASURV (Lavalley et al. 1992), the Survival Analysis package which employs the routines described in Feigelson & Nelson (1985) and Isobe et al. (1986) and evaluates differences in distributions and mean values by dealing appropriately with non-detections. The distributions for the two classes are significantly different ($P > 99.95\%$), with radio-quiet AGNs having an order of magnitude larger X-ray power for the same radio power. Fifth, for the sources for which we have a spectrum the optical classification is very different: ∼2/3 of the radio-quiet AGNs with a spectrum in Szokoly et al. (2004) are either broad-lined or high-excitation line objects, while only ∼8% of the low-power radio-loud AGNs are classified as such (one object with $P_r \sim 1.5 \times 10^{24}$ W Hz^{-1}, which is close to the dividing line with radio powerful AGNs). Finally, even though the definition of the two classes is based on their q values, the point remains that low radio power AGNs span ∼3 orders of magnitude in far-IR to radio flux density ratios (see Figure 14), meaning that their radio emission goes from being related to star formation to having a likely jet origin. Figure 14 shows also that this is not the case for high-power ($P_r \gtrsim 3 \times 10^{24}$ W Hz^{-1}) AGNs, since they basically all have $q \lesssim 1.7$ or upper limits above this value.

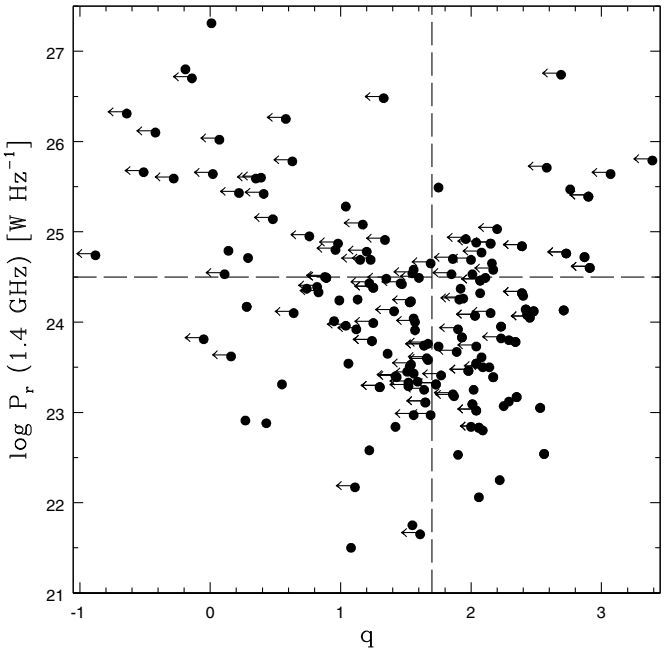

Figure 14. Radio power vs. q, the logarithm of the ratio between far-IR and radio powers for AGNs in our sample. The vertical dashed line indicates $q = 1.7$, the dividing value between radio-quiet and radio-loud AGNs, while the horizontal dashed line ($P_r = 10^{24.5}$ W Hz^{-1}) divides low- and high-power radio-loud AGNs. See the text for details.

5.4. Are Our Radio-quiet AGNs and SFGs Really Different Classes?

We have also identified two classes of radio sources with q values suggesting a star formation origin for their radio emission. Both classes have low R and low P_r (SFG by definition). They also evolve similarly in the radio band, have a similar slope of the LF, and the same range of q. Are we really dealing with two different classes? Again, the answer is: yes. First, they have very different ($P > 99.99\%$) distributions in IRAC flux ratios (Section 2), according to a two-dimensional K-S test, even before the few outliers were removed ($P \sim 99\%$), with radio-quiet AGNs populating the region where AGNs should be and SFGs distributed in the region where PAH- and starlight-dominated sources are expected to be. Second, despite their similar radio powers, they have very different redshift distributions ($P > 99.99\%$) and $\langle z\rangle$, 1.73 and 0.90 for radio-quiet AGNs and SFGs, respectively. Third, for the sources for which we have a spectrum, the optical classification is very different: ∼2/3 of the radio-quiet AGN with a spectrum in Szokoly et al. (2004) are either broad-lined or high-excitation line objects, while none of the SFGs are classified as such. Finally, even though the definition of the two classes is based also on their X-ray powers, the point remains that radio sources with $q \geqslant 1.7$ span almost six orders of magnitude in L_x (∼ three orders of magnitude on either side of the 10^{42} erg s^{-1} divide). This means that their X-ray emission goes from being related to star formation to having a clear AGN origin. In summary, although radio-quiet AGN and SFG radio have similar q values and other radio-related properties, in one case we are clearly dealing with an AGN while in the other we are not.

5.5. The Evolution of μJy Radio Sources

We now analyze in more detail the evolution of the various classes and compare it with previous results.

5.5.1. Star-forming Galaxies

Our results on the evolution of SFGs in the radio band, which we fitted with $P(z) \propto (1+z)^{k_L}$, $k_L = 2.89^{+0.10}_{-0.15}$ (or $k_L = 2.5^{+0.2}_{-0.3}$ from the $\langle V_e/V_a \rangle$ method) in the range $0 \lesssim z \leqslant 2.3$, agree very well with previous determinations. For example, Hopkins (2004) obtained $k_L = 2.7 \pm 0.6$ up to $z = 2$ (and constant thereafter), with a small (but not significant) component of density evolution $\Phi(z) \propto (1+z)^{0.15\pm0.60}$. To check if we could constrain a possible redshift peak in the evolution we tried a simple model of the type $P(z) = (1+z)^{k+\beta z}$, first suggested by Wall et al. (2008), which allows for a maximum in the luminosity evolution followed by a decline. We found no evidence for β being significantly different from 0, but we should stress that only two of our SFGs have $z > 2$.

Regarding other bands, Magnelli et al. (2009) have modeled the evolution of infrared luminous SFGs as a pure luminosity evolution $P(z) \propto (1+z)^{3.6\pm0.4}$ up to $z \sim 1.3$, while Magnelli et al. (2011) have derived $P(z) \propto (1+z)^{1.0\pm0.9}$ for $1.3 \lesssim z \lesssim 2.3$, which suggests a slowing down of the evolution at $z \gtrsim 1.3$ (in both cases the evidence for density evolution is not significant). If we split our sample we derive $k_L = 3.5^{+0.4}_{-0.7}$ ($\langle V_e/V_a \rangle = 0.63 \pm 0.04$, $P_{ev} = 99.98\%$) for $z \leqslant 1.3$ ($k_L = 3.1^{+0.8}_{-1.0}$ excluding the two large-scale structures) and $k_L = 1.6^{+0.6}_{-0.7}$ ($\langle V_e/V_a \rangle = 0.66 \pm 0.09$, $P_{ev} \sim 54\%$) for $1.3 \leqslant z \leqslant 2.3$, which is consistent with the IR results. In summary, although we find no significant evidence for a slowing down of the evolution at higher redshifts, such an occurrence cannot be ruled out by our data.

Our SFGs have $\langle L_{IR} \rangle \sim 5 \times 10^{11}\, L_\odot$, which is typical for luminous infrared galaxies (LIRGs; $10^{11} \leqslant L_{IR} \leqslant 10^{12}\, L_\odot$), and extend over $8 \times 10^9 \lesssim L_{IR} \lesssim 2 \times 10^{13}\, L_\odot$ (where L_{IR} refers to the 8–1000 μm range and we have used the mean value of the $L_{IR}/P_{1.4\,GHz}$ ratio given in Sargent et al. 2010 to estimate it), thereby reaching well into the ultra-luminous infrared galaxies (ULIRGs) regime ($L_{IR} > 10^{12}\, L_\odot$).

5.5.2. Radio-loud AGNs

We have found a significant difference between the evolutionary properties of low-power and high-power radio-loud AGNs, with a dividing line between the two at $P \sim 3 \times 10^{24}$ W Hz^{-1}. Namely, while low-power sources do not evolve, high-power ones anti-evolve significantly ($P \sim 99.9\%$), which indicates that they were either less numerous or less luminous in the past. This is exactly the opposite of what was found in samples at higher flux densities ($\gtrsim$1 Jy), where high-power sources exhibit a strong *positive* evolution, with low-power ones still not evolving (e.g., Urry & Padovani 1995; Jackson & Wall 1999). This difference is likely due to two factors:

1. The range of redshifts sampled in the two cases are very different. For example, while a 10^{25} W Hz^{-1} source in a sample defined by $S_{1.4\,GHz,min} \geqslant 1$ Jy can be detected only up to $z \sim 0.065$, if $S_{1.4\,GHz,min} \geqslant 100\,\mu$Jy the same source can be seen up to $z \sim 4.1$ ($\alpha_r = 0.7$). And indeed, for our high-power radio-loud AGNs $\langle z \rangle \sim 2$ (Table 2), which is where these sources are supposed to start their decline (e.g., Waddington et al. 2001).
2. A class of sources with $P \gtrsim 3 \times 10^{24}$ W Hz^{-1}, moderate luminosity evolution, and a cutoff redshift $z_{max} = 5.5$, will reach a limiting flux density $f_{min} \approx 70\,\mu$Jy (Padovani 2011). When the flux density limit S_{min} of a survey is comparable to, or even lower than, this value, the observer will start "running out" of sources and a deficit at higher redshifts will be observed. Stated differently, since at a first order $V_e/V_a \sim (S/S_{min})^{-3/2}$, in this case S/S_{min} can often be > 1, if not $\gg 1$, which translates into small values of V_e/V_a. The key assumption here is that there needs to be a redshift cutoff, as if sources were present at all redshifts then f_{min} would be tending to zero and no such effect would be present.

Note that the radio power, which separates the non-evolving from the anti-evolving radio sources coincides with the minimum power of FR II sources (e.g., Urry & Padovani 1995; Gendre et al. 2010; Padovani 2011) and radio-quasars (Padovani 2011). We then identify our low-power radio-loud AGNs with low-luminosity radio galaxies of the FR I type and the high-power ones with the FR II-like, powerful radio sources, which dominate the bright ($\gtrsim$1 mJy) radio sky, and of which we are witnessing the demise.

Sadler et al. (2007) and Donoso et al. (2009) have studied the radio evolution of luminous red galaxies up to $z = 0.7$ and 0.8, finding evidence of weak but significant positive evolution. Their samples have very little overlap with ours, as they include radio sources with $P \geqslant 10^{24.2}$–$10^{24.3}$ W Hz^{-1} and only seven ($\sim$8%) of our AGNs in this power range have $z < 0.8$ (see Figure 5). Furthermore, both studies only deal with red galaxies, while we include all radio sources. Our LF in the 0.4–0.8 redshift range is in any case fully consistent with theirs, although our uncertainties are obviously quite large, once we exclude four sources belonging to the two large-scale structures discussed in Section 5.2 and one optically compact source (which would have not been included by either of the two studies). The small, positive evolution they detect even at the lowest powers, that is between $10^{24.2}$ and $10^{25.8}$ W Hz^{-1} and $10^{24.3}$ and 10^{25} W Hz^{-1}, respectively, is consistent with these ranges encompassing the minimum value for FR II radio galaxies, which are known to evolve positively at the radio flux densities sampled by both studies (e.g., Gendre et al. 2010).

Taylor et al. (2009) have found that the number density of massive ($M_\star > 10^{11} M_\odot$) red galaxies declines with redshift as $\Phi(z) \propto (1+z)^{-1.60\pm0.14(\pm0.21)}$ for $z \leqslant 1.8$. This is tantalizingly similar to the dependence we find for our high-power radio-loud AGNs $\Phi(z) \propto (1+z)^{-1.8\pm0.6}$ over a larger redshift range (0.5–5.8). If we restrict our sample to $z \leqslant 1.8$ we still find evidence of negative evolution but not significantly so due to the smaller sample size.

5.5.3. Radio-quiet AGNs

We have estimated for the first time the evolution of radio-quiet AGNs in the radio band, modeling it as a pure luminosity evolution and obtaining $P(z) \propto (1+z)^{k_L}$, $k_L = 2.5^{+0.4}_{-0.5}$, in the range $0.2 \lesssim z \lesssim 3.9$. In the X-ray band the situation appears to be more complex, with strong evolution up to $z \sim 1$–2 (depending on luminosity) and then a slow down (e.g., Hasinger et al. 2005). As done for SFGs, we then tried a model of the type $P(z) = (1+z)^{k+\beta z}$ but our previous best fit ($k = 2.5$, $\beta = 0$) was still fully consistent with the data, although peaks at $z \approx 3$, for example, are also within the 1σ contours. Larger samples of radio-selected, radio-quiet samples will put strong constraints on the evolution of these sources, also bypassing the problems of obscuration, which plague the optical and soft X-ray bands, although source identification will require ancillary multiwavelength data, as shown in Section 2. Moreover, the surface density of our radio-quiet AGNs, $\sim$520 deg^{-2}, is

already a factor of ∼6 larger than that of one of the deepest optically selected quasar samples (∼80 deg^{-2} to $g \sim 22$; Richards et al. 2005) and only ∼1/4 of that of unabsorbed AGNs down to faint *Chandra* fluxes (∼2000 deg^{-2}; Hasinger et al. 2005). (Note however that we are sensitive to both broad- and narrow-lined AGNs, while both the optical and X-ray samples under consideration include only the former type.)

Our radio number counts are consistent with those in the hard X-ray band, as shown in Figure 4, which shows the predictions of Wilman et al. (2008), based on a conversion of the AGN X-ray LF to a radio LF, and of Paper IV, obtained from the X-ray number counts by using a typical radio-to-X-ray flux density ratio. This shows that the sources we are selecting in the radio band are the same as the X-ray emitting radio-quiet AGNs.

5.6. Comparison with the COSMOS and Deep SWIRE Field Surveys

Smolčić et al. (2009a) and Smolčić et al. (2009b) have studied the evolution of SFGs and AGNs in the radio band using 1.4 GHz VLA observations of the COSMOS 2 deg^2 field, which have a limiting flux density ∼45 μJy in the central 1 deg^2. Strazzullo et al. (2010) have studied a 1.4 GHz selected sample of radio sources in the Deep SWIRE Field (DSF), reaching a limiting flux density ∼13.5 μJy at the center of a 0.36 deg^2 area. We can then compare our results more directly with theirs, keeping in mind that both samples reach only $z = 1.3$ and that quasars, which make up $\lesssim$20% of the total, were not included in the AGN COSMOS sample.

Smolčić et al. (2009a) derived $k_L = 2.1 \pm 0.2$ or $k_L = 2.5 \pm 0.1$ for SFGs depending on the choice of the local LF, while we get $k_L = 3.5^{+0.4}_{-0.7}$ for $z \leqslant 1.3$ ($k_L = 3.1^{+0.8}_{-1.0}$ excluding the two large-scale structures). Their values are smaller than ours but not significantly so, given our relatively large uncertainties and the presence of large-scale structures in our field. Their evolution, unlike ours, however, is significantly weaker than found by Magnelli et al. (2009) in the IR band for $z \leqslant 1.3$ ($k_L = 3.6 \pm 0.4$: see Section 5.5.1). Strazzullo et al. (2010) have defined two classes of "star-forming" (blue) and "intermediate" (green) galaxies, for which they derive $k_L = 2.9 \pm 0.3$ and $k_L = 3.6 \pm 0.2$, respectively (their non-parametric results). This evolution is stronger than obtained by Smolčić et al. (2009a) but in good agreement with ours and also Magnelli et al. (2009).

Smolčić et al. (2009b) found $k_L = 0.8 \pm 0.1$ or $k_D = 1.1 \pm 0.1$ for their AGNs. For $z \leqslant 1.3$ we obtain $\langle V_e/V_a \rangle = 0.54 \pm 0.03$, indicative of slightly positive but not significant ($P_{ev} = 77\%$) evolution, with $k_L = 1.5$ and $k_D = 1.0$ (and obviously large error bars). If we exclude the two large-scale structures $\langle V_e/V_a \rangle = 0.57 \pm 0.03$, indicative of positive ($P_{ev} = 96.9\%$) evolution, with $k_L = 2.3 \pm 1.0$ and $k_D = 2.0 \pm 1.0$. These are larger than the COSMOS values but still consistent with them given our relatively large error bars. Part of the difference might also be explained by the exclusion of quasars from the COSMOS sample, as these are expected to be mostly of the radio-quite type (Paper IV) and therefore strongly evolving. Indeed, when splitting the sample into radio-quiet and radio-loud AGNs one obtains $\langle V_e/V_a \rangle = 0.69 \pm 0.06$, $k_L = 3.9^{+0.7}_{-0.9}$ ($P_{ev} \sim 96.8\%$) and $\langle V_e/V_a \rangle = 0.49 \pm 0.04$ ($P_{ev} \sim 85\%$), respectively ($\langle V_e/V_a \rangle = 0.52 \pm 0.04$ excluding the two large-scale structures). The apparently positive AGN evolution appears then to be driven by the radio-quiet sources, while the radio-loud ones do not evolve in the redshift range sampled by Smolčić et al. (2009b). This has important implications for their results, as they do not distinguish between the two classes of AGNs and use the positive evolution they found to estimate, for example, the evolution of the comoving radio luminosity density and mechanical energy output of low-radio-power AGNs. Strazzullo et al. (2010) derived $k_L = 2.5 \pm 0.3$ for their "quiescent" (red) galaxies, which they identify as AGNs, which is in good agreement with our result but significantly larger than the COSMOS value. Note that ∼40% of the AGNs in Strazzullo et al. (2010) are within 1σ of the infrared–radio correlation typical of SFGs, which shows that, like ours, about half of their AGNs *cannot* be of the radio-loud type (see also Prandoni 2010).

5.7. The Origin of Radio Emission in Radio-quiet AGNs

The mechanism responsible for the radio emission in radio-quiet AGNs has been a matter of debate since the discovery of quasars. Alternatives have included a scaled down version of the radio-loud AGN mechanism (e.g., Miller et al. 1993), star formation (e.g., Sopp & Alexander 1991), a magnetically heated corona (Laor & Behar 2008), and disk winds (Blundell & Kuncic 2007) (but see Steenbrugge et al. 2011).

Our results suggest very close ties between star formation and radio emission in radio-quiet AGNs, since their evolution is indistinguishable from that of SFGs (Section 3) and their LF appears to be an extension of the SFG LF (Section 4). Furthermore, radio emission in the two classes of AGNs is bound to have a different origin. If radio-quiet AGNs were simply "mini radio-loud" AGNs, in fact, they would have to share the evolutionary properties of the latter and their LF should also be on the extrapolation of the radio-loud one at low powers. None of these two facts is borne out by our data (see, e.g., Figure 9).

This concurs with the results of various papers over the past 20 years (e.g., Sopp & Alexander 1991; Sargent et al. 2010), which have shown that radio-quiet AGNs and SFGs have very similar far-IR-to-radio flux density ratios. Note, however, that Sanders et al. (1989) have discarded this as entirely coincidental, and similarly Kukula et al. (1998) have suggested that dust heating by the quasar and AGN-related radio emission could also conspire to make this happen. Moreover, the detection of compact, high brightness temperature cores in several radio-quiet AGNs (e.g., Ulvestad et al. 2005), which resemble those observed in radio-loud AGNs, would also argue against our results, although in some Seyfert galaxies these cores are surrounded by diffuse radio emission connected to star-forming regions (Orienti & Prieto 2010).

This suggests that AGN- and star-formation-related processes coexist in radio-quiet AGNs. Indeed, the fraction of flux density contained in the compact, central component is, on average, ∼70% for low-redshift radio-quiet AGNs (e.g., Kellermann et al. 1989; Kukula et al. 1998), which leaves some room for extended emission. If the AGN-related component is non-evolving, as appears to be the case for low-power radio-loud AGNs, while the star-formation-related one follows the evolution of SFGs, one could understand the difference between our radio-quiet AGNs, which have $\langle z \rangle \sim 1.7$, and those imaged with the VLBI, which are mostly local. In fact, since this redshift difference implies an increase by a factor ≈10–20 in the radio power related to star formation, a minor (∼1/3) extended component at $z \sim 0$ would then become dominant ($\gtrsim$3) at higher redshifts. Furthermore, it should be pointed out that no complete sample of radio-selected, radio-quiet AGNs has ever been observed at the VLBI resolution. The choice of objects that could be detected might have then led to a selection effect favoring relatively strong targets, more similar to radio-loud sources.

Richards et al. (2007) have studied a sample of 92 radio sources in the Hubble Deep Field North brighter than 40 μJy and well resolved by MERLIN and the VLA. By classifying more than 70% of them as starbursts or AGNs using radio morphologies, spectral indices, optical appearance, and rest-frame mid-IR emission, they found that the X-ray luminosity indicates the presence of an AGN in at least half of the 45 radio starbursts with X-ray counterparts. Moreover, almost all extended radio starbursts at $z > 1.3$ host X-ray selected obscured AGNs and their radio and X-ray powers are uncorrelated, which points to different emission mechanisms being at play in the two bands. These results, which associate high-redshift radio starbursts with AGNs, are fully consistent with our suggestion of a very close relationship between star formation and radio emission in our relatively high-redshift radio-quiet AGNs.

If radio emission in radio-quiet AGNs is mostly related to star formation processes, we can use the mean value of the $L_{\rm IR}/P_{1.4\,\rm GHz}$ ratio given in Sargent et al. (2010) to estimate their IR powers. Our radio-quiet AGNs have $\langle L_{\rm IR}\rangle \sim 4 \times 10^{12}\,L_\odot$, that is, well within the ULIRGs regime, and reach $2 \times 10^{14}\,L_\odot$. The star formation rates (SFRs) implied by their radio powers assuming that all radio emission is star formation related and using the relationship derived by Bell (2003), are, on average, $\sim$500 $M_\odot$ yr^{-1}, extending over the $\sim$10–20,000 $M_\odot$ yr^{-1} range. The mean value is typical of ULIRGs, while the upper end is in the hyperluminous infrared galaxies regime ($L_{\rm IR} > 10^{13}\,L_\odot$), which can reach SFRs $>$ 10,000 $M_\odot$ yr^{-1} (e.g., Rowan-Robinson & Wang 2010).

The association of ULIRGs with radio-quiet AGNs is certainly not new. Sanders et al. (1988) proposed an evolutionary connection between ULIRGs and quasars, based on the fact that all of the twelve ULIRGs in their sample displayed AGN spectra in the optical band ($\sim$2/3 of their quasars are radio-quiet). Moreover, the AGN detection rate among local ULIRGs is $\sim$70% (Nardini et al. 2010) and radio-detected ULIRGs are known to be rare locally but rapidly evolving with redshift (e.g., Mauch & Sadler 2007).

5.8. Astrophysics of μJy Sources

Fanaroff & Riley (1974) recognized that radio galaxies separate into two distinct luminosity classes, each with its own characteristic radio morphology. High-luminosity FR IIs have radio lobes with prominent hot spots and bright outer edges, while in low-luminosity FR Is radio emission is more diffuse. The luminosity distinction is fairly sharp at 178 MHz, with FR Is and FR IIs lying below and above, respectively, the fiducial luminosity $P_{178\,\rm MHz} \approx 10^{26}/(H_0/70)^2$ W Hz^{-1}. This translates at higher frequencies to $P_{1.4\,\rm GHz} \approx 3 \times 10^{25}/(H_0/70)^2$ W Hz^{-1} (assuming $\alpha_{\rm r} = 0.7$), with some dependency also on optical luminosity (Owen & White 1991) and therefore a rather large overlap. An independent separation on the basis of nuclear activity into high-excitation and low-excitation radio galaxies (HERGs and LERGs) has been proposed more recently (Laing et al. 1994). It turns out that almost all FR Is are LERGs and most FR IIs are HERGs, although there is a population of FR II LERGs as well. Observational evidence indicates that the two types of radio galaxies have intrinsically different central engines. Namely in LERGs the accretion disk, if at all present, is thought to be much less efficient than in HERGs (e.g., Chiaberge et al. 1999; Donato et al. 2004; Evans et al. 2006). This points to a large difference in accretion rates between the two classes.

Croton et al. (2006) have associated high-accretion sources, and therefore also HERGs, with their so-called quasar-mode, which they interpret as merger-driven, efficient accretion of cold disk gas, present also in radio-quiet AGNs. Low-accretion objects, i.e., LERGs, on the other hand, have been connected with the less efficient accretion of warm gas, the so-called radio-mode. The mean black hole accretion rate for the "radio-mode" is predicted to be approximately constant up to $z \approx 2$, based on a suite of semi-analytic models implemented on the output of the Millennium Run (Figure 3 of Croton et al. 2006). "Quasar-mode" accretion, on the other hand, is envisioned to be most efficient at $z \sim$ 2–4, dropping by a factor of five by $z \sim 0$. This is similar in form but somewhat weaker than the observed cosmological luminosity evolution of bright quasars in the radio, optical, and X-ray bands (e.g., Wall et al. 2005 and references therein).

As we identify our low-power radio-loud AGNs with FR Is/LERGs these would then be inefficient accretors in a "radio-mode," which would explain their lack of evolution, assuming that it is driven only by the accretion rate. We instead identify as sources in a "quasar-mode" the high-power radio-loud AGNs (which should be mostly HERGs) and the radio-quiet ones. Their different evolutions in the radio band are explained by distinct emission mechanisms and by the fact that the high radio powers of the former mean that we are seeing the effects of a high-redshift cutoff.

6. SUMMARY AND CONCLUSIONS

We have used a deep, complete radio sample of 193 objects down to a 1.4 GHz flux density of 43 μJy selected in the CDFS area to sharpen our understanding of the nature of sub-millijansky sources and to study for the first time their evolution and luminosity functions up to $z \sim 5$. Our unique set of ancillary data, which includes far-IR, near-IR, and optical observations, redshift information, and X-ray detections or upper limits for a large fraction of our sources, has allowed us to develop an unprecedented classification scheme to categorize in a robust way faint radio sources in SFGs, radio-quiet, and radio-loud AGNs. Our main results can be summarized as follows.

1. SFGs and AGNs make up an equal part of the sub-millijansky sky down to 43 μJy, with the former becoming the dominant population only below $\approx$0.1 mJy. Radio-quiet AGNs are confirmed to be an important class of sub-millijansky sources, accounting for $\sim$30% of the sample and $\sim$60% of all AGNs, and outnumbering radio-loud AGNs at $\lesssim$0.1 mJy.
2. The radio power of SFGs evolves as $(1+z)^{2.5-2.9}$ up to $z \leqslant 2.3$, their maximum redshift in our sample, in agreement with previous determinations in the radio and IR bands. Although evidence of a slowing down of the evolution at $z \gtrsim 1.3$ is not significant it also cannot be ruled out. The radio luminosity function of SFGs can be parameterized as broken power-law $\Phi(P) \propto P^{-1.3}$ and $\Phi(P) \propto P^{-3.15}$ at the faint and bright end, respectively, with a break at $P \sim 7 \times 10^{21}$ W Hz^{-1}, which is also consistent with previous derivations.
3. AGNs as a whole do not appear to evolve. However, once they are split into radio-quiet (energy budget dominated by thermal emission) and radio-loud (dominated by non-thermal, jet emission) sources the situation is very different, with the radio-quiet population evolving very significantly and similarly to SFGs and the radio-loud population displaying negative density evolution $\Phi(z) \propto (1+z)^{-1.8\pm0.4}$. The luminosity function of radio-loud AGNs, $\Phi(P) \propto$

$P^{-1.5}$, is also much flatter than that of radio-quiet AGNs, $\Phi(P) \propto P^{-2.6}$, derived here for the first time, which seems to be an extension of that of SFGs at the high power end.

4. There is a significant difference between the evolutionary properties of low-luminosity radio galaxies and radio-powerful ($P \gtrsim 3 \times 10^{24}$ W Hz^{-1}) AGNs since while the former do not evolve, the latter evolve negatively. This is exactly the opposite of what found in samples at higher flux densities ($\gtrsim$1 Jy), where high-power sources exhibit a strong positive evolution. We interpret this difference as due to the fact that we are sampling the high-power radio-loud population up to much larger redshifts ($z \gtrsim 5$) and as a result of a redshift cutoff.
5. Our results suggest a very close relationship between star formation and radio emission in radio-quiet AGNs, since their evolution and luminosity function are, respectively, indistinguishable from, and an extension of, that of SFGs. This is supported by the fact that both radio-quiet AGNs and SFGs appear to follow the "IR–radio relation" but is in contradiction with the detection of compact, high brightness temperature cores in several (mostly local) radio-quiet AGNs, similar to those observed in radio-loud ones. The coexistence of two components, one non-evolving and AGN related, and one evolving and star formation related, and selection effects in the choice of radio-quiet VLBI targets, can reconcile these apparently discrepant observational data.
6. The surface density of radio-selected, radio-quiet AGNs, $\sim$520 deg^{-2}, is already about six times larger than that of one of the deepest optically selected quasar sample and only $\sim$1/4 that of unabsorbed X-ray selected AGNs. This means that sub-millijansky radio surveys, given the appropriate ancillary multiwavelength data, have the potential of detecting large numbers of radio-quiet AGNs bypassing the problems of obscuration which plague the optical and soft X-ray bands. The radio number counts of radio-quiet AGNs are consistent with those in the hard X-ray band, which shows that the sources we are selecting are the same as the X-ray emitting radio-quiet AGNs.
7. Sub-millijansky radio surveys wanting to study the evolution of faint, *radio-loud* AGNs, need to consider that a large fraction ($\sim$60% down to $\sim$50 μJy) of the radio-selected AGNs are actually of the *radio-quiet* type and therefore need to be treated separately. This has not been done so far by other studies and can have a large impact on the study of faint "radio-mode" inefficient accretors.

We plan to expand on this work by using our deeper radio observations (Miller et al. 2008; N. Miller et al. 2011, in preparation) and the recently released 4 Ms *Chandra* data (Xue et al. 2011). This will provide us with a catalog of $\sim$900 radio sources, with which we will be able to address the issues discussed in this paper with larger statistics. Much larger samples will be made available by the Square Kilometre Array pathfinders (e.g., Padovani 2011) including the Evolutionary Map of the Universe survey (Norris et al. 2011) with its very large coverage ($\sim$3/4 of the sky), and the Expanded Very Large Array with its unprecedented sensitivity.

N.M. acknowledges the support of a Chandra Award AR8-9016X. P.T. acknowledges support from the ASI–INAF I/009/10/0 grant. We thank Evanthia Hatziminaoglou for useful discussions and Mark Dickinson and the FIDEL Team for providing the 70 μm FIDEL image and catalog. Extensive use was made of the TOPCAT software package (Taylor 2005). We acknowledge the ESO/GOODS project for the ISAAC and FORS2 data obtained using the Very Large Telescope at the ESO Paranal Observatory under Program ID(s) LP168.A-0485, 170.A-0788, 074.A-0709, 275.A-5060, and 081.A-0525. The VLA is a facility of the National Radio Astronomy Observatory which is operated by Associated Universities, Inc., under a cooperative agreement with the National Science Foundation. This research has made use of the NASA/IPAC Extragalactic Database (NED) which is operated by the Jet Propulsion Laboratory, California Institute of Technology, under contract with the National Aeronautics and Space Administration and NASA's Astrophysics Data System (ADS) Bibliographic Services.

Facilities: VLA, ESO:3.6m (EFOSC2), VLT:Kueyen (FORS1), VLT:Antu (FORS2, ISAAC), Max Planck:2.2m (WFI), *CXO*, *XMM*, *Spitzer* (IRAC, MIPS)

REFERENCES

Avni, Y., & Bahcall, J. N. 1980, ApJ, 235, 694
Bell, E. F. 2003, ApJ, 586, 794
Blundell, K. M., & Kuncic, Z. 2007, ApJ, 668, L103
Cardamone, C. N., Urry, C. M., Damen, M., et al. 2008, ApJ, 680, 130
Cardamone, C. N., van Dokkum, P. G., Urry, C. M., et al. 2010, ApJS, 189, 270
Chiaberge, M., Capetti, A., & Celotti, A. 1999, A&A, 349, 77
Condon, J. J. 1989, ApJ, 338, 13
Croton, D. J., Springel, V., White, S. D. M., et al. 2006, MNRAS, 365, 11
Dale, D. A., Helou, G., Contursi, A., Silbermann, N. A., & Kolhatkar, S. 2001, ApJ, 549, 215
Damen, M., Labbé, I., van Dokkum, P. G., et al. 2011, ApJ, 727, 1
Dasyra, K. M., Yan, L., Helou, G., et al. 2009, ApJ, 701, 1123
Donato, D., Sambruna, R. M., & Gliozzi, M. 2004, ApJ, 617, 915
Donoso, E., Best, P. N., & Kauffmann, G. 2009, MNRAS, 392, 617
Evans, D. A., Worrall, D. M., Hardcastle, M. J., Kraft, R. P., & Birkinshaw, M. 2006, ApJ, 642, 96
Fanaroff, B. L., & Riley, J. M. 1974, MNRAS, 167, 31p
Fasano, G., & Franceschini, A. 1987, MNRAS, 225, 155
Fazio, G., Hora, J. L., Allen, L. E., et al. 2004, ApJS, 154, 10
Feigelson, E. D., & Nelson, P. I. 1985, ApJ, 293, 192
Gehrels, N. 1986, ApJ, 303, 336
Gendre, M. A., Best, P. N., & Wall, J. V. 2010, MNRAS, 404, 1719
Gilli, R., Cimatti, A., Daddi, E., et al. 2003, ApJ, 592, 721
Hasinger, G., Miyaji, T., & Schmidt, M. 2005, A&A, 441, 417
Hatziminaoglou, E., Pérez-Fournon, I., Polletta, M., et al. 2005, AJ, 129, 1198
Helou, G., Soifer, B. T., & Rowan-Robinson, M. 1985, ApJ, 298, L11
Hopkins, A. M. 2004, ApJ, 615, 209
Isobe, T., Feigelson, E. D., & Nelson, P. I. 1986, ApJ, 306, 490
Isobe, T., Feigelson, E. D., Akritas, M. G., & Babu, G. J. 1990, ApJ, 364, 104
Jackson, C. A., & Wall, J. W. 1999, MNRAS, 304, 160
Kellermann, K. I., Fomalont, E. B., Mainieri, V., et al. 2008, ApJS, 179, 71 (Paper I)
Kellermann, K. I., Sramek, R., Schmidt, M., Shaffer, D. B., & Green, R. 1989, AJ, 98, 1195
Kukula, M. J., Dunlop, J. S., Hughes, D. H., & Rawlings, S. 1998, MNRAS, 297, 366
Lacy, M., Storrie-Lombardi, L. J., Sajina, A., et al. 2004, ApJS, 154, 166
Laing, R. A., Jenkins, C. R., Wall, J. V., & Unger, S. W. 1994, in ASP Conf. Ser. 54, The First Stromlo Symposium: The Physics of Active Galaxies, ed. G. V. Bicknell, M. A. Dopita, & P. J. Quinn (San Francisco, CA: ASP), 201
Laor, A., & Behar, E. 2008, MNRAS, 390, 847
Lavalley, M., Isobe, T., & Feigelson, E. 1992, ASP Conf. Ser. 25: Astronomical Data Analysis Software and Systems I, ed. D. M. Worrall, C. Biemesderfer, & J. Barnes (San Francisco, CA: ASP), 245
Machalski, J., & Condon, J. J. 1999, ApJS, 123, 41
Magnelli, B., Elbaz, D., Chary, R. R., et al. 2009, A&A, 496, 57
Magnelli, B., Elbaz, D., Chary, R. R., et al. 2011, A&A, 528, A35
Mainieri, V., Kellermann, K. I., Fomalont, E. B., et al. 2008, ApJS, 179, 95 (Paper II)
Marshall, H. L., Avni, Y., Tananbaum, H., & Zamorani, G. 1983, ApJ, 269, 35
Mauch, T., & Sadler, E. M. 2007, MNRAS, 375, 931
Merloni, A., Rudnick, G., & Di Matteo, T. 2008, in Relativistic Astrophysics and Cosmology—Einstein's Legacy, ESO Astrophysics Symposia (Springer: Berlin), 158

Middelberg, E., Deller, A., Morgan, J., et al. 2011, A&A, 526, A74
Miller, N. A., Fomalont, E. B., Kellermann, K. I., et al. 2008, ApJS, 179, 114
Miller, P., Rawlings, S., & Saunders, R. 1993, MNRAS, 263, 425
Morris, S. L., Stocke, J. T., Gioia, I. M., et al. 1991, ApJ, 380, 49
Nardini, E., Risaliti, G., Watabe, Y., Salvati, M., & Sani, E. 2010, MNRAS, 405, 2505
Norris, R. P., Hopkins, A. M., Afonso, J., et al. 2011, PASA, in press
Orienti, M., & Prieto, M. A. 2010, MNRAS, 401, 2599
Owen, F. N., & White, R. A. 1991, MNRAS, 249, 164
Padovani, P., Giommi, P., Landt, H., & Perlman, E. S. 2007, ApJ, 662, 182
Padovani, P. 2011, MNRAS, 411, 1547
Padovani, P., Mainieri, V., Tozzi, P., et al. 2009, ApJ, 694, 235 (Paper IV)
Prandoni, I. 2010, ISKAF2010 Science Meeting, published online at http://pos.sissa.it/cgi-bin/reader/conf.cgi?confid=112, 47
Press, W. H., Flannery, B. P., & Teukolsky, S. A. 1986, Numerical Recipes. The Art of Scientific Computing (Cambridge: Cambridge Univ. Press)
Richards, G. T., Croom, S. M., Anderson, S. F., et al. 2005, MNRAS, 360, 839
Richards, A. M. S., Muxlow, T. W. B., Beswick, R., et al. 2007, A&A, 472, 805
Rowan-Robinson, M., & Wang, L. 2010, MNRAS, 406, 720
Sadler, E. M., Cannon, R. D., Mauch, T., et al. 2007, MNRAS, 381, 211
Sadler, E. M., Jackson, C. A., Cannon, R. D., et al. 2002, MNRAS, 329, 227
Sajina, A., Lacy, M., & Scott, D. 2005, ApJ, 621, 256
Sanders, D. B., Phinney, E. S., Neugebauer, G., Soifer, B. T., & Matthews, K. 1989, ApJ, 347, 29
Sanders, D. B., Soifer, B. T., Elias, J. H., Neugebauer, G., & Matthews, K. 1988, ApJ, 328, L35
Sargent, M. T., Schinnerer, E., Murphy, E., et al. 2010, ApJS, 186, 341
Schmidt, M. 1968, ApJ, 151, 393
Seymour, N., Dwelly, T., Moss, D., et al. 2008, MNRAS, 386, 1695
Silverman, J. D., Mainieri, V., Salvato, M., et al. 2010, ApJS, 191, 124
Smolčić, V., Schinnerer, E., Scodeggio, M., et al. 2008, ApJS, 177, 14
Smolčić, V., Schinnerer, E., Zamorani, G., et al. 2009a, ApJ, 690, 610
Smolčić, V., Zamorani, G., Schinnerer, E., et al. 2009b, ApJ, 696, 24
Sopp, H. M., & Alexander, P. 1991, MNRAS, 251, 14P
Steenbrugge, K. C., Jolley, E. J. D., Kuncic, Z., & Blundell, K. M. 2011, MNRAS, 413, 1735
Stern, D., Eisenhardt, P., Gorjian, V., et al. 2005, ApJ, 631, 163
Strazzullo, V., Pannella, M., Owen, F. N., et al. 2010, ApJ, 714, 1305
Szokoly, G. P., Bergeron, J., Hasinger, G., et al. 2004, ApJS, 155, 271
Taylor, M. B. 2005, in ASP Conf. Ser. 347, Astronomical Data Analysis Software and Systems XIV, ed. P. Shopbell, M. Britton, & R. Ebert (San Francisco, CA: ASP), 29
Taylor, E. N., Franx, M., van Dokkum, P. G., et al. 2009, ApJ, 694, 1171
Tozzi, P., Mainieri, V., Rosati, P., et al. 2009, ApJ, 698, 740 (Paper III)
Treister, E., Virani, S., Gawiser, E., et al. 2009, ApJ, 693, 1713
Ulvestad, J. S., Antonucci, R. R. J., & Barvainis, R 2005, ApJ, 621, 123
Urry, C. M., & Padovani, P. 1995, PASP, 107, 803
Vardoulaki, E., Rawlings, S., Simpson, C., et al. 2008, MNRAS, 387, 505
Waddington, I., Dunlop, J. S., Peacock, J. A., & Windhorst, R. A. 2001, MNRAS, 328, 882
Wall, J. V., Jackson, C. A., Shaver, P. A., Hook, I. M., & Kellermann, K. I. 2005, A&A, 434, 133
Wall, J. V., Pope, A., & Scott, D. 2008, MNRAS, 383, 435
Wilman, R. J., Miller, L., Jarvis, M. J., et al. 2008, MNRAS, 338, 1335
Xue, Y. Q., et al. 2011, ApJS, 195, 10